33RD CONGRESS
OF THE INTERNATIONAL COUNCIL
OF THE AERONAUTICAL SCIENCES
STOCKHOLM, SWEDEN, 4-9 SEPTEMBER, 2022

ICAS 2022 SWEDEN

KNOWLEDGE-BASED CONCEPTUAL DESIGN METHODS FOR GEOMETRY AND MASS ESTIMATION OF RUBBER AERO ENGINES

Jannik Häßy[1] & Jens Schmeink[1]

[1]German Aerospace Center (DLR), Institute of Propulsion Technology

Abstract

The efficiency but also the dimensions and mass of aero engines have a significant impact on the components, drag and consumed block fuel of the aircraft. The interdependencies between the engine and the aircraft have to be accounted for to find the optimal engine in a multidisciplinary overall aircraft design process. One approach to do this, is the application of a rubber engine model that provides a broad range of different engine designs. However, to create a rubber engine model, the geometry and mass of various engines have to be predicted with sufficient accuracy during conceptual design, when only limited computation time and a small amount of data are available. Therefore, a knowledge-based method for the estimation of engine geometry is developed that utilizes an advanced parameterization of turbo components based on B-splines. The knowledge is extracted from cross-sectional drawings of existing engines that serve as reference. The geometry estimation requires thermodynamic cycle data and is combined with published component-based and part-based procedures to predict the engine mass. This combination of models enables the holistic assessment of interdependencies between thermodynamics, geometry and mass of aero engines on conceptual design level. As a validation case, a generic geared turbofan similar to the PW1100G-JM is modeled and both mass estimation methods are benchmarked. The mass breakdown of the part-based approach is compared to published data. In addition, an analysis of trends is conducted to investigate how the estimates for geometry and mass adapt to design variations. Therefore, the major design variables bypass ratio, thrust, overall pressure ratio and turbine temperature are varied. Their impact on geometry and mass is discussed and the resulting trends are compared to a published correlation-based model.

Keywords: aero engine, geometry, mass, rubber engine, conceptual design

1. Introduction

Aviation research faces major challenges in order to reduce fuel consumption, emissions and climate impact. Besides the investigation of concepts that improve the engine or aircraft in isolation, it is necessary to estimate the potential for savings arising from multidisciplinary design analysis and optimization (MDAO) of the overall aircraft system considering interdependencies. The aircraft design, its drag and consumed block fuel are significantly influenced by the efficiency, dimensions and mass of the engines. For example, engine mass and geometry are input for the nacelle, pylon and wing design processes and implicitly influence the fuselage and landing gear as well. For the optimal choice of some engine parameters e.g. the bypass ratio of a turbofan, the assessment on the overall system level is mandatory. Improvements in fuel consumption have to be traded against losses due to additional mass and drag. Hence, in order to optimally match the engine and the aircraft, highly iterative and complex design processes arise.

Context of this Publication

The conceptual engine design can be integrated into the overall aircraft design (OAD) by means of flexible engine models (rubber engines). A rubber engine model provides different engine designs for a range of boundary conditions, requirements and design parameter values. Various approaches for rubber engine models exist and can be categorized: First, the simple statistical models, e.g. [1]. Second, the direct integration of a detailed engine design process into OAD, e.g. [2, 3]. Third, the

model-based integration of detailed data for various engine designs purely with surrogate models [4–6] or with a hybrid surrogate-based approach [7].
All approaches have in common that engine geometry and mass predictions for a range of different designs are required based on the small amount of data that is available during the conceptual design phase. Several conceptual methods for the estimation of engine geometry can be found in the literature (see section 2.1). Furthermore, the original equipment manufactures (OEM) have their long time proven in-house developments. However, several approaches are not described in detail or make substantial simplifications, e.g. the assumption of a constant hub or tip radius, which is typically not the case for modern engines. Especially, when methods are applied that calculate the mass of individual parts e.g. blades, the geometry of each stage is important.
There are different mass estimation methods for aero engines available in the public domain ranging from simple correlations to determine the overall engine mass based on a few parameters to more sophisticated part-based approaches modeling the engine components in a detailed breakdown (see section 2.2). Two methods have been identified as promising regarding the applicability in the context of this work: the component-based approach according to Sagerser et al. [13] and the part-based approach according to Pera et al. [14] and Klees et al. [15]. Both methods have been excessively used before but validation cases for the latest generation of engines are rare. Furthermore, a lot of studies dealing with engine mass employed the program WATE++ [16]. It is based on the method of [14, 15] and uses updated but partially unpublished models compared to the initial procedure [17, S. 117]. Therefore, it is of interest how accurate the baseline methodology performs when WATE++ is not available.

Research Questions

This publication addresses the following research questions:

- How can detailed engine flowpaths be predicted based on a few input parameters and a small amount of data that is available during conceptual design?
- How accurate are published methods that predict the engine mass on the basis of components and parts in case of the latest generation of geared turbofan engines? Where is potential for model improvements?
- How can interdependencies between the thermodynamic cycle, geometry and mass be accounted for in order to create rubber engine models for the application in overall aircraft MDAO?

Contribution of this Publication

This paper presents a new knowledge-based methodology to predict the two-dimensional geometry of complex engine flow paths using the knowledge about similar well known engine designs. An advanced parameterization for turbo components based on B-splines and characteristic blade parameters is developed to increase the level of detail while keeping the number of required input parameters limited. The use of splines simplifies the creation of smooth contours and steady transitions between components. The numerical procedure to generate the geometry of turbo components based on the proposed parameterization is explained in detail. Thereby, the reader will be enabled to implement the geometry generation procedure for his own software framework. In addition to the application in conceptual design, the herein described procedure can be used for geometry generation in the field of aerodynamic analysis and optimization (see e.g. [12]). Furthermore, this publication summarizes the component-based and part-based mass estimation approaches according to Sagerser et al. [13] and Pera et al. [14] to allow a direct comparison of the governing equations. Both approaches are implemented and coupled with the developed geometrical model and a material database to provide the required input parameters. The models for geometry and mass estimation are combined with the thermodynamic performance code DLRp2 to enable a holistic assessment of engine-related interdependencies. Thereby, an important capability for the provision of rubber engine models in the context of overall aircraft MDAO is described. The scope of this paper is a robust and fast assessment using a geometrical knowledge-base in combination with semi-empirical correlations and zero-dimensional thermodynamic cycle data. No aerodynamic methods e.g. meanline or through flow

approaches or detailed structure-mechanical analysis are considered in order to reduce complexity and computational time in the very early design phase. The methods are implemented as part of the virtual engine framework GTlab (Gas Turbine Laboratory) [9–11]. The resulting geometry and mass are stored using the common data model [8] of GTlab. Hence, the results from the process can be used directly as a starting point for higher-fidelity analysis. For validation, the presented methodology is used to estimate the geometry and mass of a generic geared turbofan similar to the PW1100G-JM. The component- and part-based mass estimation approaches are benchmarked. The mass breakdown generated with the part-based method is analyzed in detail and compared to published data. The disk masses of the PW1100G are approximated and an updated disk correlation is derived for the validation case. Then, a design study is performed in order to assess the applicability of the presented methodology in the context of MDAO using a rubber engine model approach. Therefore, the major design variables thrust, overall pressure ratio (OPR), bypass ratio (BPR) and turbine stator outlet temperature (T_{41}) are varied. The impact of design changes on engine geometry and mass is analyzed and the resulting trends are discussed.

2. State of the Art

In this section, methods for geometry and mass estimation of aero engines as well as application cases are summarized. In this field, a lot of studies have been published and this paper does not claim to give a complete overview. The main focus lies on conceptual design methods that model the engine on the level of components or parts.

2.1 Engine Geometry Estimation

The estimation of engine geometry and mass is closely connected in the literature, . Most of the detailed approaches for mass estimation also have a geometrical model since the prediction of engine mass usually requires information on the actual dimensions. For the engine diameter and length, very simple scaling laws based on statistical correlations utilizing the parameters thrust and bypass ratio are presented in [1]. Sagerser et al. developed simple equations to calculate the length of components for lift and cruise engines using correlations for characteristic geometrical parameters [13]. The more detailed approaches model the 2D-geometry of the engine annulus. The methods published by Pera et. al [14] and Klees et al. [15] lays the basis for programs like WATE++ [16] and ATLAS [17]. Futhermore, the OEM's have internal developments, which are not described in detail but are applied in published studies [6, 18, 19]. For preliminary design, a detailed geometrical model of the core engine is presented in [20]. The use of Bézier curves and splines for geometry parameterization has the potential to describe complex geometries based on a few degrees of freedom. For example, splines are utilized to describe the hub and tip contour of compressors in the context of aerodynamic optimization in [21, 22].

2.2 Engine Mass Estimation

In the following, a brief overview of existing mass estimation methods for the conceptual design of gas turbine aero engines with focus on the more detailed approaches is given. A detailed summary of publicly available methods including a broad range of simple correlation-based methods can be found in [17, 23]. Principally, three different categories of mass estimation approaches during the conceptual design phase can be distinguished. The complexity of the methods and the required inputs increase significantly with the level of detail. The 'overall engine' correlations predict the total engine mass based on one or a few parameters and no further mass breakdown is available. The 'component-based' methods predict the mass of single turbo components of the engine and require much more input parameters. The 'part-based' approaches determine the mass of single parts of a turbo component. Summing up all part masses leads to the component mass. The part-based methods require the most input parameters and detailed geometrical models. The classification of a method may be contradictory sometimes. For example, the 'component-based' method of Sagerser et al. [13] do not consider individual masses for structural engine components. The 'part-based' method according to Pera et al. [14] and Klees et al. [15] consider individual masses for structural components e.g. frames, shafts and ducts but do not consider single parts.

2.2.1 Overall Engine Correlations

First of all, the most simple methods correlate the overall engine mass with one or more characteristic engine parameters, e.g. mass flow, thrust, bypass ratio, diameter or overall pressure ratio [1, 24–31]. Mostly, these methods are purely statistical and based on engine data coming from a specific time frame. In [23, 32, 36], part-based methods for engine mass prediction are used to generate regression models in order to derive modern overall engine mass correlations with improved accuracy while maintaining the simple applicability with only a few input parameters. When overall engine correlations are applied, adaptions of the engine design do not change the predicted mass as long as the input values for the correlation remain equal. Therefore, correlations for the overall engine mass are not suitable for detailed conceptual design studies because they can capture design variations only with strong limitations. Furthermore, these models cannot be used for the investigation of novel engine architectures, increased technological levels, e.g. due to new materials or fabrication techniques, or new features on component level (e.g. VGV, Active clearance control) since they have been created for a specific technology and time frame.

2.2.2 Component-Based Methods

The second category comprises the component-based methods that provide mass estimates for single components of an aero engine e.g. compressors, combustor and turbines. The statistical component-based method according to Sagerser et al. [13] has been created based on data for cruise and lift engines with different development status ranging from preliminary design to production. The goal was to provide simplified mass models capturing first order effects to enable parametric studies on the propulsion system for vertical take-off and landing (VTOL) applications. But the method is applicable for both cruise and lift engines with axial flow components since correlation factors for both cases are provided. Besides correlations for turbo components, also the fan duct, combustor, accessories and structure are considered. For each component a mathematical equation that contains first-order dependencies was deduced from a simple physical analysis and the correlation factors were determined by fitting the engine data, mostly by graphical means. But there has been considerable scatter in the component data. One reason for that was the difficulty to collect the data due to different configurations, structural loads and reported breakdowns of the available propulsion systems. In addition, different design techniques and technological levels led to variations. Sagerser et al. investigated the accuracy of the approach by calculating the total mass of 14 engines that also have been used to create the correlations. It is stated that the deviations for single components partly cancel each other during the summing process which leads to a mitigated deviation in the overall engine weight. For 12 engines, the estimate showed an absolute deviation of approximately 10% or less. The range of parameters covered by the underlying engine data is specified by Sagerser et al. and it is emphasized that the correlations may produce invalid trends when they are applied outside of this range or if unusual parameter combinations are evaluated. Furthermore, it is stated that the method is rather suitable to predict relative changes when design variations are performed than to estimate the absolute engine mass.

2.2.3 Part-Based Methods

Finally, the part-based approaches consider the mass of single parts of each component, e.g. disks, blades and casing in the case of turbo components. The approach according to Pera et al. [14] enables the mass estimation of conventional and unconventional axial flow engine configurations since the mass breakdown is made on part level, which allows various engine arrangements. Statistical correlations are developed based on data from 29 engines and are combined with simple physic-based approaches e.g. the calculation of blade pull stress by considering blade geometry, material density and rotational speed. The mass estimation often considers approximations of the volume of parts, which enables the selection of different materials and the adaption to current material technology. Besides the part-based consideration of turbo components, estimation procedures for combustors, ducts, frames, shafts, nozzles, mixers, thrust reversers, heat exchangers, accessories, gears and annulus inverting valves are described. The method lays the basis for the calculation program WATE-1 (Weight Analysis of Turbine Engines) and was validated by predicting the engine mass of 8 engines whereby some of them were used to develop the method. The accuracy of the method was found to be

in the magnitude of 5%. Klees et al. [15] adapted the method for the purpose of hand calculations and introduced an improved correlation for the shaft mass that not only account for the transmitted torque but also for the effect of shaft deflection. Onat et al. [33] presented the updated program version WATE-2 that was extended by rotational moments of inertia for rotor blades and disks, center of gravity, correlations for small gas turbines including radial flow compressors and turbines as well as a physics-based disk calculation procedure. Later, Hale [34] derived the program version WATE-S that was specifically tailored to small gas turbine engines. In 2002, Tong et al. [35] presented enhancements that have been made to WATE. A major change was the introduction of an improved preliminary design procedure using finite-differences to calculate disks of different types (ring, web, hyperbolic) and a module for disk-life assessment. In 2008, Tong [16] described the conversion of WATE, which has been developed in Fortran so far, into the object-oriented program WATE++ using NPSS (Numerical Propulsion System Simulation). Greitzer et al. derived updated empirical coefficients e.g. for the blade volume factor [36, p. 135-136] by fitting these according to available engine masses and information provided by Pratt & Whitney. Lolis [17] implemented the program ATLAS as part of the TERA framework for mass estimation based on the method initially described by Pera et al. [14]. Another more detailed approach using preliminary design methods to estimate the mass of the core engine can be found in [20]. A simple scaling method to account for relative changes in engine mass is presented in [4]. There, stationary masses are correlated with their occupied volume and rotating masses are scaled with volume and rotational speed.

2.2.4 Application and Validation of Mass Estimation Methods

This section gives an overview of published validation cases for mass estimation methods and application studies.

- Lolis et al. [23] assessed the accuracy of different methods by estimating masses for up to 64 engines. Mostly, simple overall engine correlations are investigated. With the more detailed approaches of Sagerser et al. [13] seven and with the program WATE one engine is evaluated. Furthermore, WATE predictions for a variation of bypass ratio and turbine inlet temperature at cruise are presented. The resulting trends are compared to overall engine correlations. It was shown that the overall engine correlations are not suitable for preliminary design studies.
- Tong et al. made mass predictions for a turbofan similar to the GE90 engine [16, 35, 37].
- Jackson [38] used the method according to Sagerser et al. to predict the mass of the Trent 892 and V2500-A5 with an accuracy of -17 % and -24 %, respectively.
- A detailed mass breakdown for seven engines calculated with WATE++ is given in [36]. These engines include the CFM56-7B27, V2530-A5, PW2037, PW4462, PW4168, PW4090 and GE90-85B and have been used to derive updated empirical coefficients for WATE++. An accuracy of $\pm$ 10 % was found for most of the modeled engines.
- Donus et al. [19] investigated the accuracy of the MTU in-house mass estimation methods provided by the preliminary design tool MOPEDS. For fans, ducts and the combustor, the approach according to Sagerser et al. [13] is applied. In-house part-based methods are utilized for compressors and turbines. The geometry of six production engines is modeled and the relative mass breakdown into the different components is presented. The generated mass predictions are compared in an averaged form to the real component masses. For turbo components, the results are also presented for different parts, e.g. disks, blades and casing.
- Lolis [17] calculated mass estimates for the engines Trent 892 and CFM56-7B27 with ATLAS and for the CFM56-7B27 also with WATE++ in order to validate the method. The real total engine mass is predicted with an accuracy between 4.8 and 5.6 %.
- In a previous publication, Häßy et al. [7] applied the presented methodology of this paper to predict the bare engine mass of the Trent 1000 R3 with an error of 2.6 % and 7.1 % using a part-based and component-based approach, respectively.

3. Methods

In the context of this work, the virtual engine framework GTlab was extended by the developed knowledge-based procedure for geometry estimation and methods for mass prediction from the literature. GTlab [9–11] enables multidisciplinary simulations of aero engines and gas turbines at different levels of detail and is being developed at the Institute of Propulsion Technology of the German Aerospace Center (DLR). In this section, the different methodological bricks of the developed procedure for predicting geometry and mass are described. The overall process is schematically visualized in figure 1. A thermodynamic engine model and the cross-sectional drawing of a well-known real engine serve as starting points. The thermodynamic model is used to provide performance data for various sizing operating points. Besides overall key parameters such as the thrust specific fuel consumption (TSFC), this data includes e.g. mass flows, temperatures, pressures and flow areas at the inlet and outlet of each modeled component. The cross-sectional drawing of the engine annulus is used to extract geometrical characteristics of components and to create a knowledge-base. The thermodynamic cycle data and the extracted geometrical knowledge are input for the geometry generation process. The mass estimation is done using the performance data, created geometry and for each component specifically selected materials from a database.

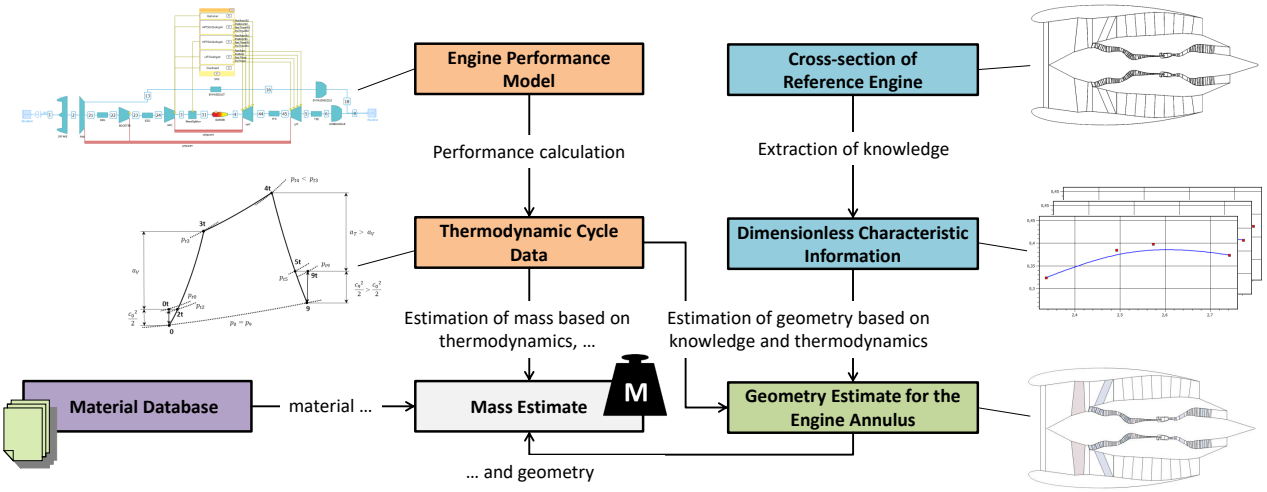

Figure 1 – Schematic overview of the geometry and mass estimation process.

3.1 Geometry Estimation

The estimation of geometry in the conceptual design phase cannot be more than a rough estimate with the aim of approximating a hypothetical detailed designed engine for the same set of boundary conditions. But the goal is to account for first order effects at this early stage of development and to produce reliable trends when major design parameters of the engine are changed. Furthermore, prediction methods for conceptual design have to be fast and robust to enable the investigation of high-dimensional parameter spaces. In order to meet this challenge, a knowledge-based approach was developed to predict the two-dimensional engine geometry. The knowledge about engine components is extracted in form of characteristic geometrical properties from the cross-sectional drawing of an existing engine (see Fig. 1). The extracted characteristic parameters constitute the knowledge-base that is then used to create similar components for changed thermodynamic cycles, requirements and boundary conditions.

3.1.1 Geometry Parameterization

The number of required parameters to describe a turbo component increases with the level of detail that is accounted for. During conceptual design, a simplified two-dimensional description is sufficient. For this publication, the leading and trailing edges of blades are considered as straight lines and the hub and tip contour of the annulus is described by a simplified smooth curve without details e.g. complex end wall shaping or sealing air injection. There are various possibilities to parameterize

turbo components. For example, in the central data model [8] of the GTlab framework, stations are used to parameterize the annulus and blades of turbo components. They are related to each other by a certain logic and are stored using the coordinates of their constituting points. Here, this parameterization is used to store the resulting geometries. But for the knowledge-base and the generation procedure, a parameterization is chosen that makes use of B-splines and mostly nondimensional characteristic blade parameters. The trajectory of the meanline and the trend of the annulus height of components are described as B-splines. The corresponding control points and knot vectors are stored in the knowledge-base. Additionally, the individual aspect ratio AR, taper ratio TR, leading edge angle α_{LE} and blade spacing factors g_{rel} are stored for each blade row considering a simplified two-dimensional blade shape. The selection of similar blade parameters for the estimation of geometry is not new (see e.g. [14, 15]). A valid set of splines and blade parameters uniquely defines the two-dimensional shape of a turbo component. One advantage of the selected parameterization is that the chosen nondimensional blade parameters do not change or vary only slightly for similarly designed components. For example, when cycle parameters and therefore the x-r-coordinates of turbo components are changed within certain limits, the aspect ratio of blades is not altered. Furthermore, the use of splines enables a continuously differentiable parameterization of arbitrary paths and complex changes can be made on the basis of a few degrees of freedom. For example, smooth transitions between the components can be achieved by adjusting the slope at the inlet and outlet.

Meanline and Annulus Height Splines

The annulus of a representative turbo component is depicted in figure 2a. The annulus height h is measured orthogonal to the meridional flow direction from the hub to the tip line. The meanline connects all points (x, r_m) that are defined at the half of the annulus height. In figure 2b, the splines for the meanline and annulus height are visualized for the representative turbo component as a function of the spline parameter t. The component inlet is located at $t = 0$ and the outlet at $t = 1$. Please note, that the spline parameter t differs from the axial coordinate x in the case of the meanline.

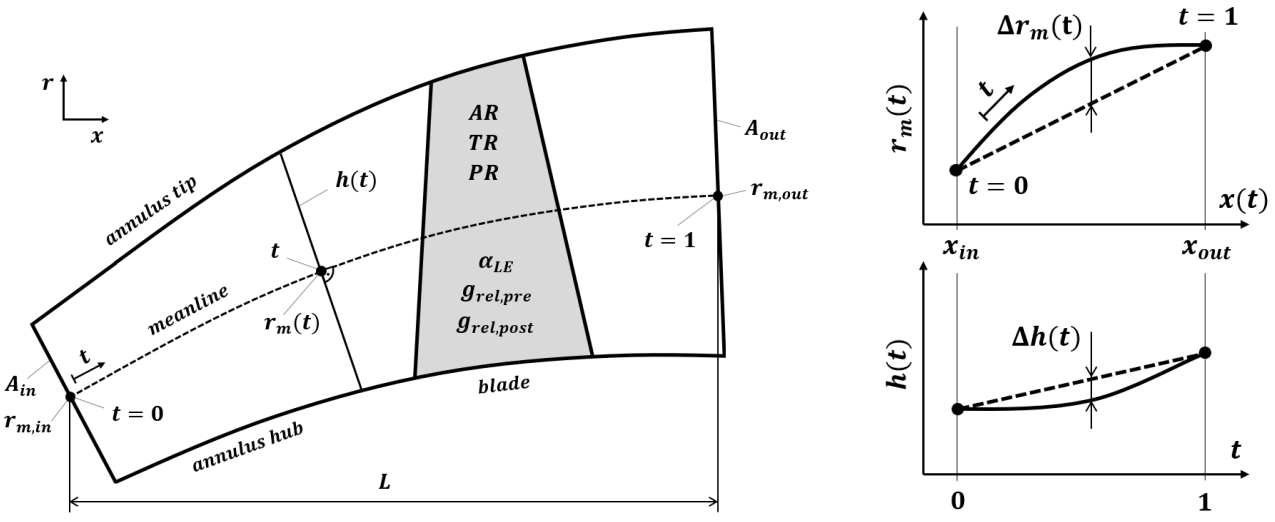

(a) Overall annulus parameter

(b) Spline definitions

Figure 2 – Parameterization of the annulus for a representative turbo component.

The meanline radius r_m and the annulus height h vary between the inlet and outlet with t. This variation leads to the characteristic hub and tip contours of the component. It is assumed that this characteristic is the same for similarly designed components with slightly different boundary conditions. But the further the design moves away from the reference that was used to generate the knowledge-base, the more uncertain this assumption becomes. To allow the adaption of the area or radius at the inlet or outlet of a component while maintaining a similar geometrical characteristic, the curve for r_m and h is split in two parts: a linear change and a nonlinear delta. When the area or radius is changed, the linear part is directly adapted. The nonlinear delta is modified according to scaling laws that will be

described in the following.

Scaling Laws

The extracted reference splines are scaled to allow the specification of different areas or annulus heights and mean radii at the inlet and outlet. In the following, the scaling procedure is described. The extracted data from the well-known engine is referred to as 'reference' and the resulting geometry from the process as 'scaled'. The relative position in the annulus f_x with respect to the axial coordinate x is defined as

$$f_x(t) = \frac{x_{ref}(t) - x_{ref,in}}{x_{ref,out} - x_{ref,in}} \tag{1}$$

whereby only the unscaled reference splines are evaluated. The factor

$$f_r = \frac{L}{L_{ref}} = \frac{x_{out} - x_{in}}{x_{ref,out} - x_{ref,in}} \tag{2}$$

describes the length of the scaled component relative to the reference component. This factor does not depend on the spline parameter t but, as will be described later, the component length L has to be found iteratively. The axial position in the annulus for a given value of t is then

$$x(t) = x_{in} + f_x(t)\, L \tag{3}$$

The mean radius considering only the linear change can be calculated as

$$r_{m,linear}(t) = r_{m,in}\ (1 - f_x(t)) + r_{m,out}\ f_x(t) \tag{4}$$

for both the reference and scaled component using the corresponding values for r_m at the inlet and outlet. For the reference spline, the nonlinear change of the annulus mean radius can be expressed as

$$\Delta r_{m,ref}(t) = r_{m,ref}(t) - r_{m,ref,linear}(t) \tag{5}$$

The mean radius of the scaled component as a function of the spline parameter t is then

$$r_m(t) = r_{m,linear}(t) + f_r\ \Delta r_{m,ref}(t) \tag{6}$$

whereby the nonlinear part is scaled with f_r. This keeps the characteristic of the meanline similar to the reference when the component length changes. In order to scale the annulus height h at given spline parameter t, the linear part

$$h_{linear}(t) = h_{in} + t\ (h_{out} - h_{in}) \tag{7}$$

can be evaluated for the reference and the scaled component with the corresponding values at the inlet and outlet. The nonlinear part is defined as

$$\Delta h_{ref}(t) = h_{ref}(t) - h_{ref,linear}(t) \tag{8}$$

and is related to the total annulus height to derive the factor

$$f_h(t) = \frac{\Delta h_{ref}(t)}{h_{ref,linear}(t)} \tag{9}$$

Finally, the annulus height of the scaled component as a function of the spline parameter t is

$$h(t) = h_{linear}(t)\ (1 + f_h(t)) \tag{10}$$

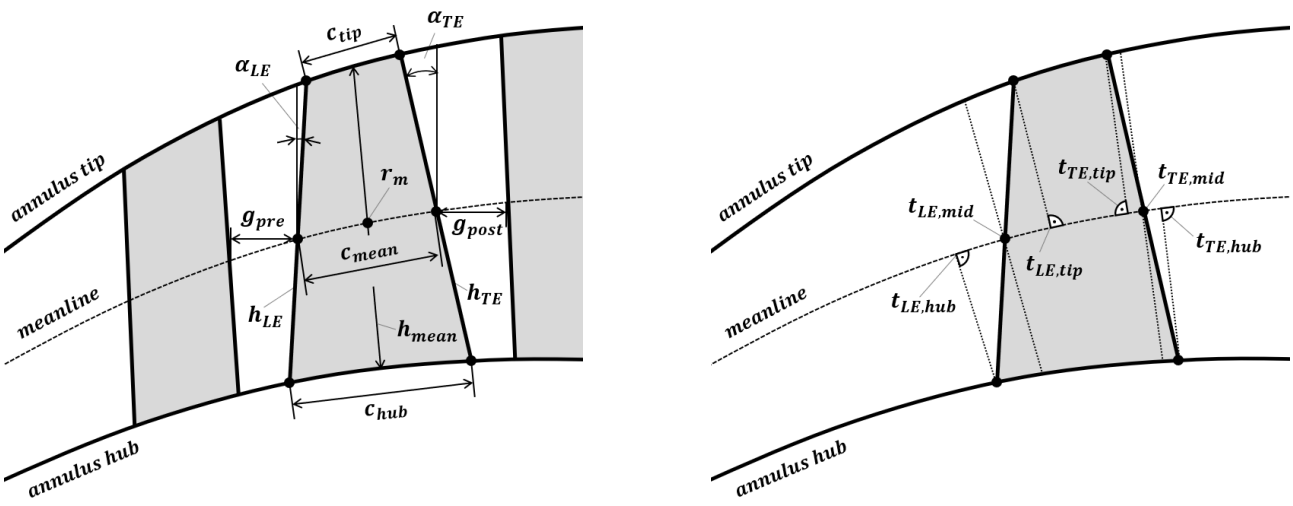

(a) Definition of blade parameters

(b) Definition of the spline parameters for the leading and trailing edge of blades

Figure 3 – Parameterization of the blades for a representative turbo component.

Blade Parameters

For each blade, individual parameters are given in the knowledge-base. For the definition of geometrical parameters, only a two-dimensional view is considered and no effects due to blade twist are accounted for. In Figure 3a, the definitions of chord length, blade height, gaps and blade angles are shown. With these definitions, the axial aspect ratio (AR) is defined as

$$AR = \frac{h_{mean}}{c_{mean}} \tag{11}$$

and the axial taper ratio (TR) of rotors and stators as

$$TR_{Rotor} = \frac{c_{tip}}{c_{hub}} \qquad \text{and} \qquad TR_{Stator} = \frac{c_{hub}}{c_{tip}} \tag{12}$$

The axial pitch ratio (PR), which is the reciprocal value of the blade solidity, is calculated with the number of blades (N_B) as

$$PR = \frac{2\,\pi\,r_m}{N_B\,c_{mean}} \tag{13}$$

and the relative blade spacing factor

$$g_{rel,i} = \frac{g_i}{c_{mean}} \tag{14}$$

relates the axial gap between blade rows at the meanline to the meridional chord of the blade. It is important to be aware of these simplified definitions, when a comparison with higher-fidelity models that include the effect of twist is made.

3.1.2 Geometry Generation Procedure

A parameter set consisting of areas and radii at the inlet and outlet, splines, blade parameters and the stage count uniquely define the component's geometry. In the following, the numerical procedure to derive the two-dimensional geometry in form of x-r-coordinates based on the previously described parameterization is explained. Here, the aim is to provide sufficient details to enable the reader to implement the procedure for his own software framework. However, not all implementation details can be shown due to space limitations.

Solving Strategy

The geometry generation is formulated as a fixed-point iteration in equation 15. The vector $\vec{x}_k$ contains the axial length of the component and the spline parameters $t_{LE,i}$ and $t_{TE,i}$ at the leading and trailing edge of the blades where m is the total number of blade rows of the current component. The sequence is converged when the function f_1 maps $\vec{x}_k$ to itself allowing a certain tolerance. Then, with $\vec{x}_{fix}$ the valid geometry of the current component is found.

$$\vec{x}_{k+1} = \begin{pmatrix} t_{LE,mid,1} \\ \vdots \\ t_{LE,mid,m} \\ t_{TE,mid,1} \\ \vdots \\ t_{TE,mid,m} \\ L \end{pmatrix} = f_1(\vec{x}_k) \tag{15}$$

$$\text{with } \vec{x}_{fix} = f_1(\vec{x}_{fix}) \text{ and } k \in \mathbb{N}_0,\ f_1 : \mathbb{R}^n \to \mathbb{R}^n,\ n = 2m+1,\ t_{LE,mid,i} \in [0,1],\ t_{TE,mid,i} \in [0,1]$$

For each evaluation of the function f_1 another mathematical problem is solved separately for each blade row. For each of the m blade rows, the mean chord c_{mean} (see Fig. 3a) and the spline parameters that define the hub and tip points t_i (see Fig. 3b) are found to fulfill equation 16. Then, the resulting blade geometry matches the specified parameters AR^*, TR^* and α^*_{LE} taken from the knowledge-base and has straight leading and trailing edges that connect the corresponding hub and tip points.

$$f_2(\vec{y}_j) = \vec{z}_j \stackrel{!}{=} \vec{0}$$

$$\text{with } \vec{y}_j = \begin{pmatrix} c_{mean} \\ t_{LE,tip} \\ t_{LE,hub} \\ t_{TE,tip} \\ t_{TE,hub} \end{pmatrix},\ \vec{z}_j = \begin{pmatrix} AR - AR^* \\ TR - TR^* \\ \alpha_{LE} - \alpha^*_{LE} \\ \alpha_{LE,tip} - \alpha_{LE,hub} \\ \alpha_{TE,tip} - \alpha_{TE,hub} \end{pmatrix} \tag{16}$$

$$\text{and } j \in \{1, ..., m\},\ f_2 : \mathbb{R}^5 \to \mathbb{R}^5$$

The presented problem formulation was chosen because it was found to be very robust and simplifies the analysis of errors since a row-wise calculation divides the geometry generation process in several small problems. An alternative problem formulation that leads to an increased convergence rate and less computational effort may be possible. But since the implementation is sufficiently fast and divergence problems are rare, no attempt is made to investigate alternative solutions. A flow chart that visualizes the solving strategy for the geometry problem is depicted in figure 4. A separate execution of this process is required for each component. The process solves the mathematical problem that is formulated in equations 15 and 16 iteratively. In the following, the single steps of the procedure are explained.

Step 1: Initialize Spline Scaling

During the thermodynamic cycle analysis, flow areas at the inlet and outlet of the component are calculated based on assumed meridional Mach numbers. The radial inlet and outlet position of the component is specified by means of hub-to-tip ratios and meanline radius ratios. These prescribed areas and radii are then used to initialize the scaling laws of the meanline and annulus height splines. Thereby, it is ensured that the created geometry matches the prescribed conditions at the inlet and outlet. For the conversion of the flow area to the annulus height, the lateral surface area of a right circular conical frustum is considered which leads to equation 17.

$$A = 2\pi r_m h \tag{17}$$

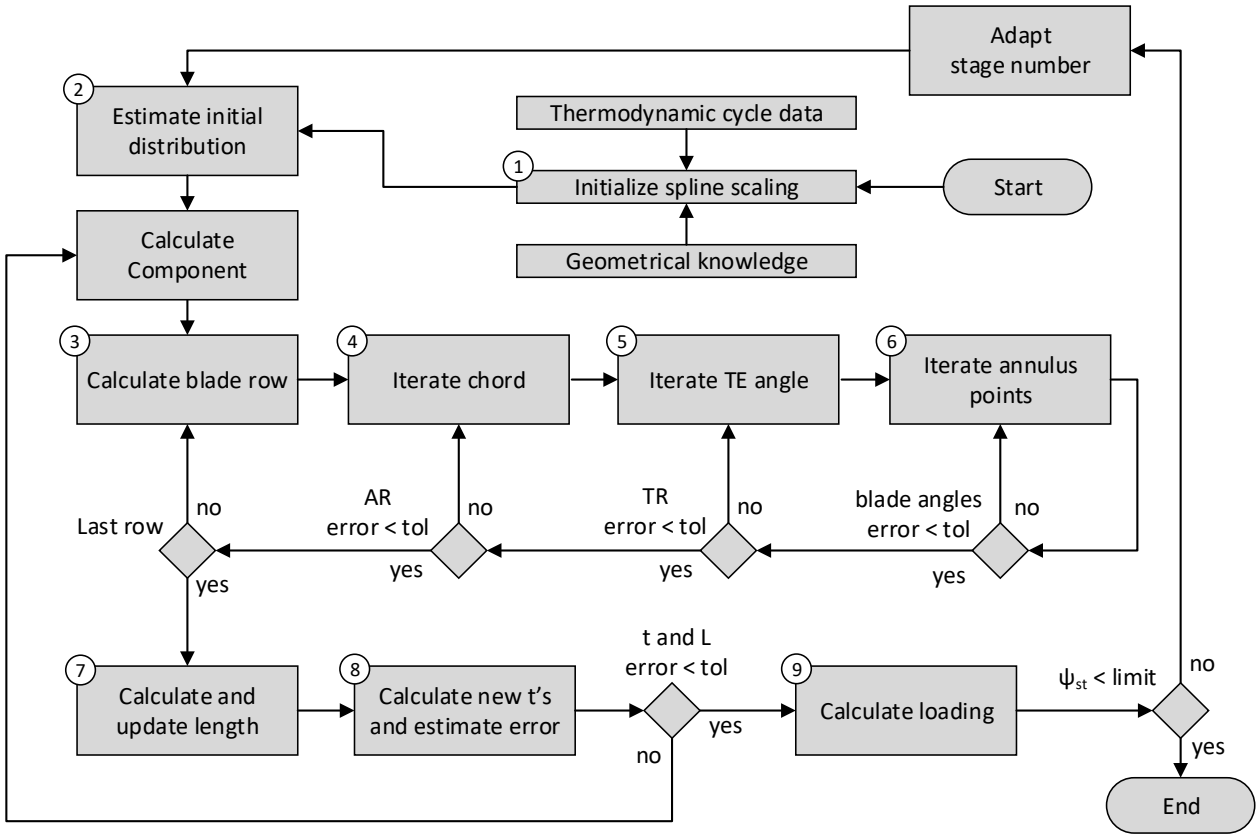

Figure 4 – Flow chart to visualize the geometry generation process.

Step 2: Initial Guess

In order to start the iterative calculation procedure, an initial guess $\vec{x}_0$ is required. Therefore, start values are estimated for the component length and the spline parameters $t_{LE,mid,i}$ and $t_{TE,mid,i}$ that define the distribution of blade edges along the component. In the authors implementation, the start values for t_i are distributed evenly between 0 and 1 according to the number of blade rows and an approximated relative spacing factor g = 0.3. The component length can be initially guessed taking into account the number of blade rows, the annulus height at the inlet and outlet and a mean blade aspect ratio.

Step 3: Calculate Blade Row

For the steps 3 to 6, the parameters in $\vec{x}_k$ remain unchanged until they are updated during steps 7 and 8. For constant parameters in $\vec{x}_k$, the blade rows are calculated one by one, starting with the first row. The axial position of the row upstream is input for the calculation of the neighboring row downstream. For each row, the prescribed aspect ratio AR^*, taper ratio TR^* and leading edge angle α^*_{LE} of the blades are taken from the knowledge-base. When the targeted number of stages differs from the reference geometry, the second last stage is copied or removed. The last stage often has certain characteristics that should be maintained. The annulus height h_i as well as the radius of the meanline points $r_{m,i}$ at the leading and trailing edge come from an evaluation of the scaled splines using the spline parameters $t_{LE,mid}$ and $t_{TE,mid}$, respectively. For each row, the problem in equation 16 is solved separately. Therefore, a nested loop approach was chosen that comprises the steps 4 to 6. As result, the hub and tip points of the row are defined and the next blade row is calculated until all rows have been considered.

Step 4: Iterate Chord

At the top level of the nested loop approach, the chord of the considered row is varied until the prescribed aspect ratio of the blade is reached (see Fig. 5a). The corresponding chord length is

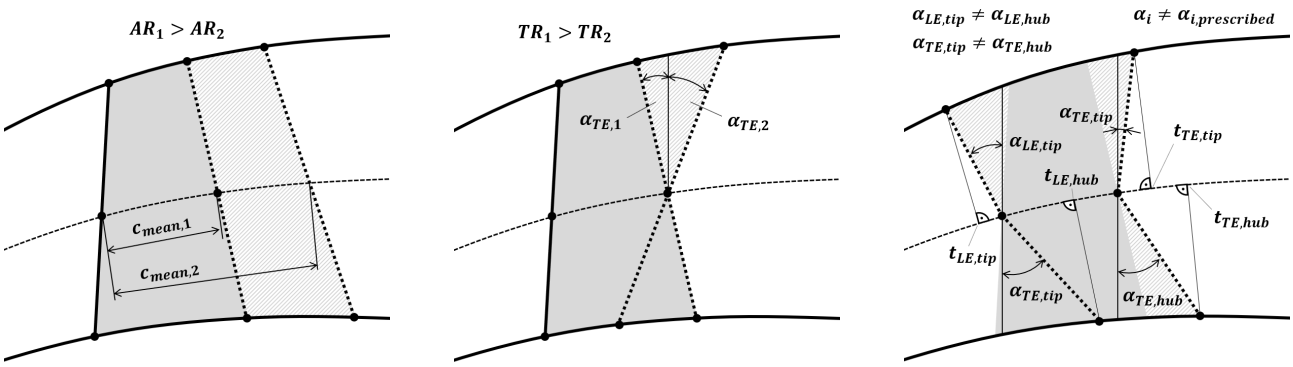

(a) Step 4: Iterate chord (b) Step 5: Iterate TE angle (c) Step 6: Iterate annulus points

Figure 5 – Visualization of the steps 4, 5 and 6 for blade geometry generation.

calculated with a root-finding algorithm. Therefore, the Newton approach and as a fallback solution the Brent algorithm is applied. Each evaluation of step 4 includes full convergence of the subordinate steps 5 and 6. In contrast to the radial coordinate $r_{m,i}$ of the meanline points at the leading and trailing edge, the axial coordinate x_i of these points is not taken from the evaluation of the meanline spline. The axial coordinate of the currently considered blade row's leading edge $x_{LE,i}$ results from the axial coordinate of the trailing edge of the upstream row $x_{TE,i-1}$ and the blade gap g_i. The blade gap is the maximum gap value considering both blade rows. Therefore, the relative blade spacing factors $g_{rel,i}$ that are taken from the knowledge-base are applied. Then, the axial coordinate of the current blade trailing edge $x_{TE,i}$ results from the leading edge position $x_{LE,i}$ and the chord length. Thus, there is a mismatch in the axial coordinates x_i between the calculated values and the values that result from an evaluation of the meanline spline with $t_{LE,mid}$ and $t_{TE,mid}$ from $\vec{x}_k$. This subtle difference is neglected in figure 5a but will be important for step 8.

Step 5: Iterate TE Angle

On the second level, the trailing edge angle α_{TE} is varied until the prescribed taper ratio TR^* is reached (see Fig. 5b). The Brent algorithm is used to solve this root-finding problem. Step 6 is brought to convergence for each execution of step 5.

Step 6: Iterate Annulus Points

On the last level of the nested loop approach, the spline parameters $t_{LE,tip}$, $t_{LE,hub}$, $t_{TE,tip}$ and $t_{TE,hub}$ are determined to match the prescribed leading and trailing edge angles in the hub and tip region (see Fig. 5c). Therefore, four root-finding problems are solved with the Brent algorithm. A linear extrapolation of the meanline and annulus height spline with $t < 0$ and $t > 1$ is utilized to ensure feasible solutions especially close to the inlet and outlet of the component.

Step 7: Calculate and Update Length

When all rows are calculated, the component length, which is the axial distance between the meanline points at the inlet and outlet, is determined for $\vec{x}_{k+1}$ and the scaling laws are updated. The component length L is part of the scaling laws (see Eq. 2, 3 and 6). Hence, the coordinates of a meanline point for a constant spline parameter t change when L is updated.

Step 8: Calculate New Set of Spline Parameters

In the description of step 3, the mismatch between the axial meanline coordinates x_i of blade edges and the values that would result from the evaluation of the meanline spline is mentioned. In addition, the updated component length in step 7 leads to changed coordinates (x_i, $r_{m,i}$) coming from the evaluation of the meanline spline with unchanged spline parameter values in $\vec{x}_k$. In order to match the blade coordinates of the meanline points with the scaled meanline spline, the fixed-point iteration is applied. The values of the meanline spline parameters $t_{LE,mid,i}$ and $t_{TE,mid,i}$ that would result in the calculated axial coordinates of the created blades are estimated and thereby, a new set of spline parameters is

generated for $\vec{x}_{k+1}$ in equation 15. With these new values and the updated axial component length, the procedure is repeated until the fixed-point iteration converges. Then, the mismatch between the blade coordinates and the spline evaluation is vanished.

Step 9: Calculate Loading

After the successful calculation of the turbo component, the average stage loading

$$\psi_{st} = \frac{1}{N_r} \sum_{i=1}^{N_r} \frac{\Delta h_i}{U_{m,i}^2} \tag{18}$$

is estimated for a specified operating condition where N_r is the number of rotors. The parameter U_m is the circumferential velocity at the meanline of the currently considered rotor and Δh is the total enthalpy that is added by the rotor assuming an equal distribution over the stages. When ψ_{st} exceeds a prescribed limit $\psi_{st,max}$, an additional stage becomes necessary. Then, the stage count is adapted and the hole process is executed again. In the implementation for this paper, it is also checked whether a reduction in stage count with respect to the maximum allowed stage loading is possible.

Increase Speed and Robustness

In order to accelerate the convergence of the fixed-point iteration, a good set of start values can be generated by a fast assessment with blade parameter iterations turned off. With the resulting length and blade distribution in $\vec{x}_{fix}$, the process is rerun with all iterations turned on. In some cases, it is necessary to add a sort of numerical damping to avoid divergence. Therefore, the length update in step 7 is done using an average value $L_{k+1} = \frac{1}{2}\left(L^*_{k+1} + L_k\right)$.

Example Geometries

Geometry estimates for a intermediate pressure compressor (IPC) and a low pressure turbine (LPT) with different number of stages are depicted in figure 6 to give an example of resulting geometries. Only the stage count varies and all other geometrical input parameters are identical.

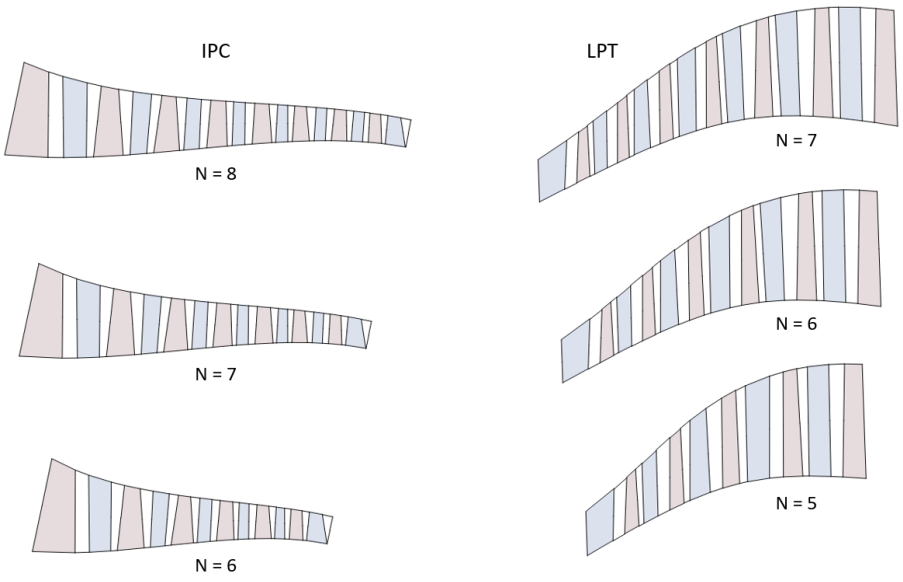

Figure 6 – Some examples for component geometries with different stage count but otherwise identical input parameters.

Overall Engine Geometry

The estimation of duct geometries follows a similar procedure. The geometry model for the combustor is described in [9]. Finally, when all individual geometries for turbo components, ducts and the combustor are generated, these are combined to form a consistent two-dimensional engine annulus (see Fig. 9 in section 4.2).

3.2 Mass Estimation

In the conceptual design phase, only a few characteristic parameters of the engine are known and no details about parts are available. Hence, the mass estimation is inevitably subject to uncertainty at this point. Furthermore, the actual mass of fully designed engines depends not only on the technology level and characteristic thermodynamic parameters but also on design heuristics. For example, different design philosophies of OEM's can lead to scatter in mass since different engineering solutions are found for the same design task. The purpose of mass estimation methods in conceptual design is the correct and consistent indication of trends when designs variations are made. For the mass estimation, the component-based method according to Sagerser et al. [13] and the part-based method of Pera et al. [14] and Klees et al. [15] are implemented. In the following, the most relevant equations of both approaches are presented in order to reveal the fundamental physical dependencies, to give the reader an insight into the complexity of the approaches and to allow a direct comparison. The methods are supplemented by a statistical gearbox correlation [39] and a model to approximate the casing thickness by considering blade-off events [20]. All masses are calculated in kg and the input parameters are in SI units unless otherwise stated.

3.2.1 Component-based Mass Estimation

This section presents an overview of the equations for the component-based mass estimation for cruise engines according to Sagerser et al. [13].

Fan

The fan mass includes the rotor and stator as solid titanium blades, spinner, hub contour wall, outer case and structure in the bypass section for the transmission of loads. The fan mass is calculated by

$$M_{Fan} = K_f \, D_t^{2.7} \frac{N_{st}}{\sqrt{\overline{AR}}} \left(\frac{S_t}{S_{t,ref}} \right)^{0.3} \left(\frac{U_{t,max}}{U_{t,ref}} \right)^{0.3} \tag{19}$$

where $K_f = 135$ is an empirical coefficient, D_t the fan tip diameter, N_{st} the stage number and $\overline{AR}$ the averaged axial aspect ratio of the rotor blades. The blade tip solidity S_t and maximum circumferential velocity $U_{t,max}$ are related to typical reference values of 1.25 and 350 $\frac{m}{s}$, respectively.

Compressor

The compressor mass model accounts for blades, disks, seals and casing. The total mass is

$$M_{Compressor} = K_c \left(r_{m,in} + r_{m,out} \right)^{2.2} N_{st}^{1.2} \left(\frac{U_{t,max}}{U_{t,ref}} \right)^{0.5} \left(1 + \frac{L/D}{L/D_{ref}} \right) \tag{20}$$

with K_c = 24.2, $U_{t,ref} = 335 \frac{m}{s}$ and the ratio of the compressor length to inlet mean diameter L/D with $L/D_{ref} = 0.2 + 0.081 N_{st}$. For boosters, Sagerser et al. suggested to calculate the first two stages with equation 19.

Combustor

The case, liner and fuel injection devices are considered for the the combustor mass

$$M_{Combustor} = K_b \left(r_{m,in} + r_{m,out} \right)^2 \left(\frac{L/H}{L/H_{ref}} \right)^{0.5} \tag{21}$$

where K_b = 390 and L/H is the ratio of axial length to the passage height with L/H_{ref} = 3.2.

Turbine

The turbine mass model accounts for blades, disks, the sealing and casing with

$$M_{Turbine} = K_t \left(r_{m,in} + r_{m,out} \right)^{2.5} N_{st} \, U_m^{0.6} \tag{22}$$

where K_t = 7.9 and $U_m = \pi \, n_{max} \left(r_{m,in} + r_{m,out} \right)$ is a mean circumferential velocity calculated with the maximum rotational speed n_{max}.

Structure and Accessories

The mass of structural components that include engine mounts, bearings, shafts and ducts is calculated by relating it to the total component mass

$$M_{Structure} = K_s \left[\sum_j M_{Fan,j} + \sum_j M_{Compressor,j} + \sum_j M_{Combustor,j} + \sum_j M_{Turbine,j} \right] \tag{23}$$

with K_s = 0.18. For the accessories of cruise engines Sagerser et al. specify a range from 9 to 30 % of the total bare engine mass. Here, a value of 15 % is assumed following the assumptions of Greitzer et al. [36, p. 140].

3.2.2 Part-based Mass Estimation

In this section, the governing equations for the part-based approach according to Pera et al. [14] and Klees et al. [15] are briefly summarized. The total mass of turbo components results from the summation of the individual masses of blades, disks, the casing and connecting hardware. The bare engine mass further includes the combustor, ducts, frames, shafts, gearbox and accessories.

Blades

The metal volume of one blade V_B is defined as

$$V_B = K_v \frac{h_{mean}^3}{AR^2} = K_v \, h_{mean} \, c_{mean}^2 \tag{24}$$

with the empirical blade volume factor K_v. This factor describes the volume fraction of the blade material in a rectangular cuboid around the blade that has the height h_{mean} and a quadratic base with side length c_{mean}. Pera et al. and Klees et al. specify typical values of K_v for different component types that account for fire-tree blade foots, effects due to twist and typical ranges of thickness-to-chord ratio. Please note, K_v is a nondimensional coefficient and do not need a conversion of units (see [15, p. 7]). The blade volume factor K_v represents a specific technology level and more recently published coefficients can be found in [36, p. 136]. With the selected material and its density ρ_B as well as the number of blades N_B of the considered row, the total blade mass

$$M_B = V_B \, \rho_B \, N_B \tag{25}$$

is found. The number of blades is calculated during the geometry generation process by means of the prescribed axial pitch ratio PR that is taken from the knowledge-base (see Eq. 13). The number of blades is always rounded up to an integer value. Pera et al. assume equal geometry and mass for rotors and stators but here both are calculated individually.

Disks

For the assessment of the disk mass, the root blade pull stress σ_{root}

$$\sigma_{root} = \frac{\rho_B \, U_{tip}^2}{g \, TR_{3D}} \left[\frac{1-\nu^2}{2} + \frac{TR_{3D}-1}{12} (1-\nu)(1+3\,\nu) \right] \tag{26}$$

is considered where ν is the hub-to-tip ratio of the blade and g is the gravitational acceleration. The blade tip speed $U_{tip} = 2\,\pi\, n_{max}\, r_t$ for the operating condition with the maximum rotational speed n_{max} is considered. For the calculation of the blade pull stress the taper ratio TR_{3D} that accounts for twist has to be used and here TR_{3D} = 1 is assumed due to the lack of more detailed information on the blade shape. Pera et al. developed correlations for different disk types that connect the disk volume V_D, rotor hub radius r_h and the blade pull stress at the blade root σ_{root}. Curves that describe the relative disk thickness $t_{Disk,rel}$

$$t_{Disk,rel} = \frac{V_D}{r_h^2} = f(\sigma_{Disk,rel} = \sigma_{root}\, r_h) \tag{27}$$

as a function of the relative disk load per unit thickness $\sigma_{Disk,rel}$ are taken from [15, p. 11] and are depicted in figure 7a. The correlation was developed using data that showed significant scatter and

only trends with an accuracy of ± 30 % can be expected for the corresponding level of technology [15, p. 11]. The correlations were created for a yield strength of 827 MPa. Klees et al. suggests to scale the abscissa with the ratio of yield strengths when other disk materials are assumed [15, p. 11]. This is important since modern disks made of titanium-based or nickel-based alloys have improved strength capabilities. Furthermore, the correlation of the type 'Titanium Compressor Disk' is not used here because it is assumed that modern titanium alloys have increased strengths and the distinction in [14, p. 18] has become obsolete. Instead, the type 'Steel Compressor and Turbine Disk' is applied. The disc mass M_D is then calculated with the material density according to equation 28.

$$M_D = r_h^2 \, t_{Disk,rel} \, \rho_D \tag{28}$$

Please note, the disk mass assessment is based on semi-empirical correlations. These have been fitted to scattered data that is representative for a specific level of technology. Here, this method is also applied for more modern engines due to its simplicity and in order to keep complexity limited. A more physics-based procedure for disk calculation using finite-differences was presented by Tong et al. [35].

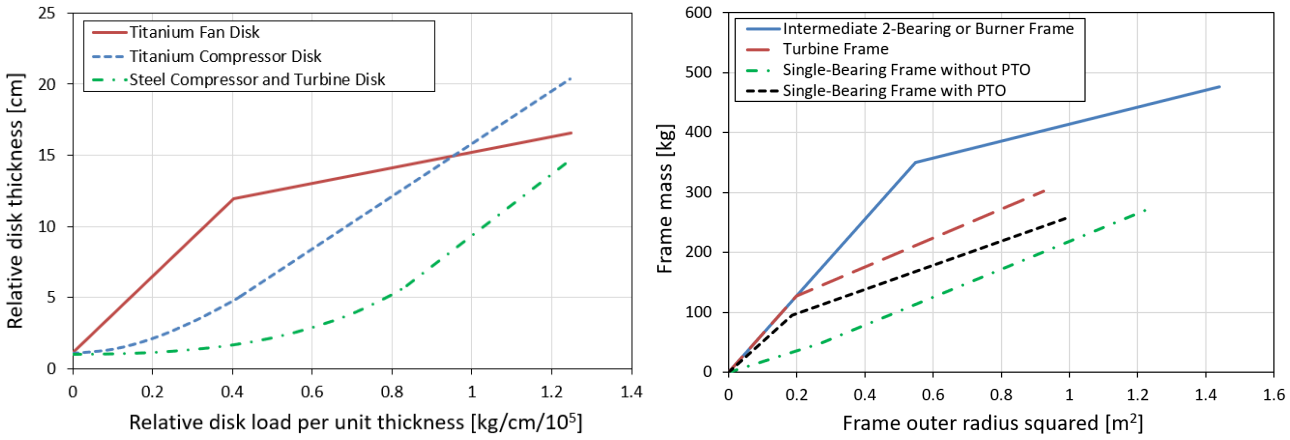

(a) Disk thickness

(b) Frame mass

Figure 7 – Correlations for disks and frames according to [15].

Casing

The casing of real engines is rather complex and consists of several parts. For example, turbine casings are usually double-walled, contain flow paths for secondary air as well as sealing devices and might have active clearance control. Compressors, especially the rear part of HPCs, often have double-walled cases and complex features e.g. devices for variable stator vanes or flow paths for secondary air extraction. Here, the casing is modeled as a simple single-walled geometrical envelope of the flow path with an averaged thickness. For both compressors and turbines, the casing thickness is determined by considering a blade-off scenario. The casing must have sufficient strength to contain a lost blade. In order to approximate the required wall thickness, the approach according to Fedortschenko et al. as it is described in [20, p. 58-62] is applied. The maximum impact stress for the casing τ_{max} is

$$\tau_{max} = 0.65 \, \mu \, \frac{\sigma_{case,max}}{S} \tag{29}$$

where $\sigma_{case,max}$ is the maximum allowable stress (yield strength) for the selected material and the empirical coefficient for consolidation is set to μ = 1.3. In this publication, the safety factor S = 2 is introduced to maintain a sufficient safety margin to the event of casing punctuation by an impacting blade. The kinetic energy of one blade $E_{kin,max}$ at maximum rotational speed n_{max} is approximated by

$$E_{kin,max} = \frac{1}{2} \frac{M_B}{N_B} \left(2 \, \pi \, n_{max} \, r_{COG}\right)^2 \tag{30}$$

with the radial coordinate of the center of gravity of the blade $r_{COG} \approx r_{mean}$. The tip perimeter l_p accounts for the contact area between the blade tip and the casing when it comes to an impact.

$$l_p = 2\,c_{tip}\,(1+d) \tag{31}$$

For this paper, the profile thickness related to the chord length at the tip is assumed to be d = 0.04 and d = 0.2 for compressors and turbines, respectively. Then, the required casing thickness t_{case} that already includes a safety margin is calculated as

$$t_{case} = C_{case}\sqrt{\frac{E_{kin,max}}{\tau_{max}\,(\iota+\lambda+\frac{\kappa}{2})\,l_p}} \tag{32}$$

with the empirically defined parameters ι = 0.7, λ = 0.05 and κ = 2.5 that account for the fractions of ductile, elastic and shear deformation energy, respectively [20, p. 61]. The empirical factor C_{case} is used for calibration. A value of C_{case} = 1.0 is assumed for compresses and turbines of the core engine as it is suggested in [20, p. 62]. The required thickness is calculated for each row and then an average value is assumed for the whole casing of the component. For the fan rotor containment, the factor C_{case} = 1.0 leads to unrealistic thick walls and has to be calibrated according to a reference. The fan case is often thinner offside the rotor containment region and have to be reduced e.g. in the region of the bypass stators. In order to calculate the casing mass M_C, the tip contour of turbo components is divided into segments and all segment masses are summed up.

$$M_{CA} = \sum_j 2\,\pi\,r_j\,l_j\,t_{case}\,\rho_{case} \tag{33}$$

where r_j is the mean radius and l_j the length of the casing segment j. In equation 33, the lateral surface area of a right circular conical frustum is multiplied with the casing thickness and the material density.

Connecting Hardware

The hardware that connects the disks of a turbo component is considered stage-wise as a cylinder with the thickness t_{con}. The total mass is then

$$M_{CO} = \sum_j 2\,\pi\,r_{h,j}\,\frac{r_{con}}{r_h}\,l_{con,j}\,t_{con}\,\rho_D \tag{34}$$

where $l_{con,j}$ is the distance between the disks, $r_{h,j}$ is the blade hub radius and the same material as for the disks is assumed. The factor $\frac{r_{con}}{r_h}$ that describes the relative location of the connection is set to 0.75 and the thickness t_{con} to 0.075 inch according to [14, p. 18].

Combustor

The combustor mass $M_{Combustor}$ includes the casing, liner and miscellaneous hardware e.g. fuel manifold and injector (see Eq. 35, according to [15]). The first term approximate the liner and casing as simple cylinders with an averaged thickness t_l = 1.4 mm [15, p. 14] and t_c = 8 mm (assumption). The radii r_o and r_i are the outer and inner radius of the combustor casing, respectively. For equation 35, the radial distance between the casing and the liner is assumed to be the same on both sides.

$$M_{Combustor} = 2\,\pi\,(r_o+r_i)\,(t_c+t_l)\,L\,\rho + C_{misc}\,\pi\,(r_o^2-r_i^2)\,L \tag{35}$$

L is the axial length and ρ the material density of the combustor. The second term accounts for the miscellaneous hardware. The approximated combustor volume is multiplied with the empirical coefficient $C_{misc} = 293.41\ \frac{kg}{m^3}$ taken from [15, p. 14] in compliance with unit conversion.

Ducts

Here, the mass of the hub and tip annulus walls of ducts is calculated in analogy to equation 33 with a prescribed wall thickness. Pera et al. and Klees et al. suggest to calculate the wall thickness based on the pressure difference between the working fluid and the ambient, which leads to thin walls.

Frames

Frames transfer forces from the shafts and bearings to the outer case of the engine. These structural elements have a high share of the total engine mass. Pera et al. created correlations for different types of frames [14, p. 35]: Frames that support the bearing of one shaft are of the type 'single-bearing' and can have an integrated shaft for power off-take (PTO). This frame type is used in the compression section of the engine. The 'double-bearing' frames are imposed to the forces of two shafts and are used in the intermediate region of the engine at inter-compressor ducts or the combustor. The 'turbine' frame is used for bearing support at inter-turbine ducts in the hot section. The frame mass M_F for the different types is correlated with the squared outer frame radius r_F, which is proportional to the frame projected area (see Fig. 7b).

$$M_F = f(r_F^2) \tag{36}$$

In the implementation for this publication, frames of the type 'double bearing' with power off-take are modeled by adding the difference in mass between the single-bearing curves in order to account for the integration of the off-take shaft. The selection of the number and type of the frames for a modern or future engine might be difficult sometimes because the bearing concepts have changed since the publication of the correlation in 1977. In the case of fans, the outer frame radius r_F is assumed to be located at the hub of the bypass stators. It is assumed that from there the forces are mainly transmitted by the stator blades to the fan casing.

Shafts

The shaft mass M_S is roughly estimated according to [15, p. 15] by

$$M_S = C_{shaft} \sqrt[3]{\frac{P_W}{n}} L_{shaft}^3 \tag{37}$$

with the empirical coefficient for steel $C_{shaft} = 4.36 \times 10^{-6} \, \frac{kg}{cm^3} \sqrt[3]{\frac{rpm}{kW}}$ and the shaft length L_{shaft}. For the transferred shaft power P_W and the rotational speed n, the maximum power condition is considered.

Gearbox

The mass of the gearbox including the lubrication system M_{GBX} is estimated by means of the empirical correlation according to Hendricks et al. [39].

$$M_{GBX} = C_{GBX,1} + C_{GBX,2} \left(\frac{P_W}{n} \right)^{0.75} \left(i_{GBX} \right)^{-0.15} \tag{38}$$

where P_W is the maximal transferred power, n is the corresponding rotational speed of the output shaft and the empirical coefficients are $C_{GBX,1} = -16.976 \, kg$ and $C_{GBX,2} = 52.766 \, kg \, \frac{rpm}{hp}^{0.75}$.

Accessories

According to [15, p. 16], the engine accessories e.g. oil, fuel, ignition, anti-icing systems make up 10 % of the bare engine mass excluding accessories. Here, a value of 15 % is assumed following the assumptions of Greitzer et al. [36, p. 140].

4. Validation Case

A two-spool unmixed geared turbofan engine serves as a validation case for the entire process that includes geometry and mass estimation. The generic engine model has a single-stage fan, which is connected to the low-pressure (LP) shaft via a gearbox. In addition to the fan, the LP shaft drives a three-stage fast-running booster. The required power is extracted from the hot gas by a three-stage fast-running low-pressure turbine (LPT). The high-pressure (HP) system is composed of a compressor (HPC) with 8 stages, a combustor and a two-stage turbine (HPT). The components are connected by inter-compressor ducts (ICD) and one inter-turbine duct (ITD). The turbine exhaust case (TEC) at the hot end completes the core section.

4.1 Assumptions for the Generic Engine Model

A thermodynamic performance model that covers all relevant operating points is created and the characteristic performance parameters are shown in table 1. The generic model is similar to the PW1100G-JM and was calibrated with respect to certification data that is available to the public domain in the ICAO Aircraft Engine Emissions Database [40]. A comparison of the fuel flow and thrust specific fuel consumption (TSFC) at sea level static between the generic model and the PW1100G-JM data is presented in figure 8.

Table 1 – Characteristic performance parameters of the generic geared turbofan model.

Parameter	Unit	Cruise	Top of Climb	Max. Takeoff	End of Field
Flight Mach Number	*[-]*	0.78	0.78	0.0	0.25
Altitude	*[m]*	10668	10668	0.0	11
Inlet Mach Number	*[-]*	0.630	0.684	0.560	0.588
Inlet Massflow	*[kg/s]*	242.9	247.9	578.4	618.5
Thrust	*[kN]*	22.8	27.6	147.3	147.3
TSFC	*[g/kNs]*	14.07	14.48	7.11	9.75
OPR	*[-]*	37.5	43.0	38.0	38.5
BPR	*[-]*	11.6	10.9	10.7	10.9
Fan Pressure Ratio	*[-]*	1.41	1.47	1.41	1.42
T_3	*[K]*	744	811	900	912
T_{41}	*[K]*	1471	1619	1759	1779

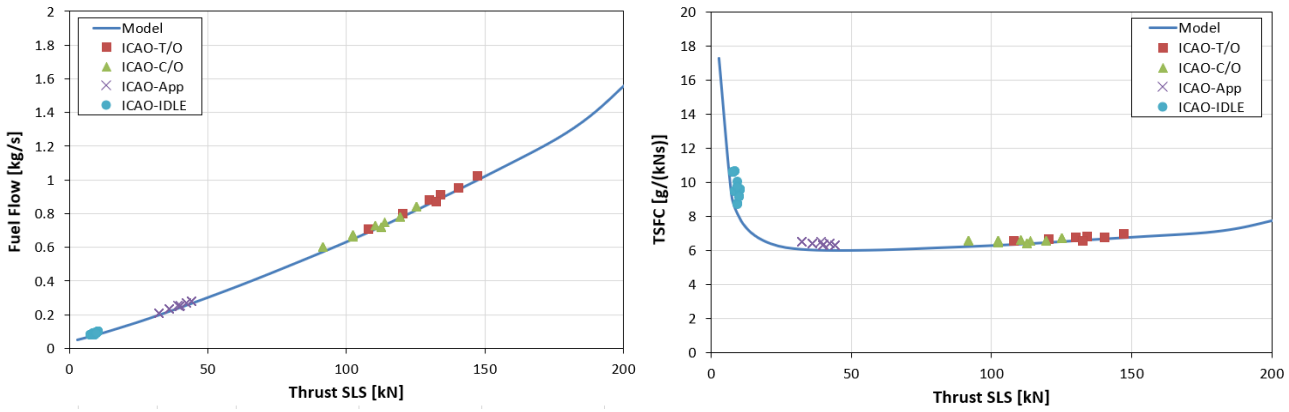

(a) Fuel flow

(b) Thrust specific fuel consumption (TSFC)

Figure 8 – Comparison of the generic model to the ICAO data of the PW1100-JM.

The characteristic geometrical information on the validation engine that builds the knowledge-base is extracted component-wise from the cross-sectional drawing of a PW1100G published in [41]. It is assumed that the drawing shows only an interim state of the engine. Therefore, the drawing is scaled to meet the publicly available geometrical dimensions of the PW1100G-JM. The fan tip diameter is 2.057 m according to [42] and the overall engine length measured from the fan spinner face to the aft flange of the TEC is 3.40 m [43]. The extracted geometrical parameters are subject to uncertainty due to the limited resolution of the drawing. Nevertheless, the geometrical data is assumed to be similar to the PW1100G. The generated set of geometrical information and the calculated thermodynamic data are then used as input for the geometry generation process. An overview of selected input parameters for geometry and mass estimation is given in table 2.

Mostly nondimensional input parameters are chosen for the calculation of the generic engine model. This allows design variations that lead to feasible engine geometries on conceptual level in section 5., where the same set of input parameters is used. The Mach number XM_i at the inlet and outlet of each component is calculated for cruise conditions according to the thermodynamic cycle and the extracted areas from the reference drawing. The inlet radius of turbo components is specified by means of the hub-to-tip ratio ν_i. For the outlet, the radius ratio $\frac{r_{m,out}}{r_{m,in}}$ is used to ensure reasonable component scaling. For the HPT there is an exception and the ratio of the HPC outlet to the HPT inlet is used to specify the

Table 2 – Overview of selected input parameters for geometry and mass estimation.

Parameter	Unit	Fan	ICD 1	Booster	ICD 2	HPC	Combustor	HPT	ITD	LPT	TEC
XM_{in}	*[-]*	0.630	-	0.412	-	0.515	-	0.098	-	0.317	-
XM_{out}	*[-]*	0.520	-	0.446	-	0.293	-	0.505	-	0.550	0.719
ν_{in}	*[-]*	0.282	-	0.705	-	0.515	-	1.139*	-	0.750	-
$r_{m,out}$ / $r_{m,in}$	*[-]*	-	-	0.906	-	1.111	-	0.982	-	1.476	0.923
$\psi_{st,max}$	*[-]*	-	-	0.25	-	0.38	-	-	-	1.50	-
$K_{v,rotor}$	*[-]*	0.055	-	0.120	-	0.120	-	0.156	-	0.195	-
$K_{v,stator}$	*[-]*	0.055	-	0.120	-	0.120	-	0.576	-	0.195	-
C_{case}	*[-]*	0.47	-	1.0	-	1.0	-	1.0	-	1.0	-
$t_{case,tip}$	*[mm]*	0.007	0.007	-	0.007	-	0.008	-	0.010	-	0.007
$t_{case,hub}$	*[mm]*	0.007	0.003	-	0.003	-	0.008	-	0.003	-	0.003
Blade Material		Ti-17	-	Ti-17	-	Inconel 718	-	CMSX-10	-	Inconel 718	-
Disk, Case Material		Ti-17	Ti-17	Ti-17	Ti-17	Inconel 718	Hastelloy X	Waspaloy	Inconel 718	Inconel 718	Inconel 718
Frame Type		Double-Bearing	-	-	Single-Bearing PTO	-	-	-	Turbine Frame	-	Single-Bearing

* ratio of mean inlet radius of the HPT and the mean outlet radius of the HPC

inlet radius instead of ν_{in}. This ensures a similar radial arrangement of the HPC and HPT compared to the reference geometry even if cycle parameters are varied. The ducts are created to match the inlet and outlet planes of the turbo components. The stage count is calculated in order to keep the loading at cruise below the prescribed limit $\psi_{st,max}$. It is assumed that the HPT always has two stages. The empirical blade volume factors are taken from [15, p. 7]. The more recently published values for K_v [36, p. 136] are not applied here since for fans only a broad range is specified. Furthermore, K_v was reduced by 77 % for the LPT to K_v = 0.045 for which no comprehensible justification was provided. The casing thickness t_{case} of turbo components is calculated according to equation 32. In case of the fan, the rotor containment thickness t_{case} = 13.6 mm is approximated based on the drawing [41] and the corresponding calibration factor C_{case} = 0.47 is calculated to reach that thickness for the validation case. For ducts (including the fan core and bypass) as well as the combustor, the thickness is roughly approximated based on the available drawing.

Table 3 – Assumptions for material properties.

Material	Unit	Ti-17	Inconel 718	Hastelloy X	CMSX-10	Waspaloy
Density	*[kg/m³]*	4650	8260	8210	9020	8190
Yield Strength	*[MPa]*	1030	1280	360	900	795

For the LP components of the compression section, titanium-based alloys are assumed as material. Nickel-based alloys are selected for the HPC and the components of the hot section. The assumed material properties are given in table 3. Four frames are considered to transfer mechanical loads to the outer case. The LP shaft is supported by a fan frame at the front and the TEC frame at the rear. The fan frame has the type 'Double-Bearing' because it is imposed to forces from the bearings in front of and after the gearbox. The TEC frame has the type 'Single-Bearing' because it supports only the LP shaft. For the HP shaft, the intermediate frame with a power off-take shaft is located at the ICD2 and has the type 'Single-Bearing PTO'. In the hot section, a frame of the type 'Turbine' is modeled at the first stator of the LPT.

4.2 Geometry Estimation

Figures 9 and 10 show the predicted engine geometry for the generic engine model. The engine annulus (see Fig. 9) matches well with the overall geometry of the PW1100G from [41] that was used to create the geometrical knowledge-base. There might be large deviations on blade level especially for the HPC and HPT due to the limited resolution of the published drawing. Typical 'dummy' blades are assumed for each component to visualize the geometry in 3D showing the calculated blade count.

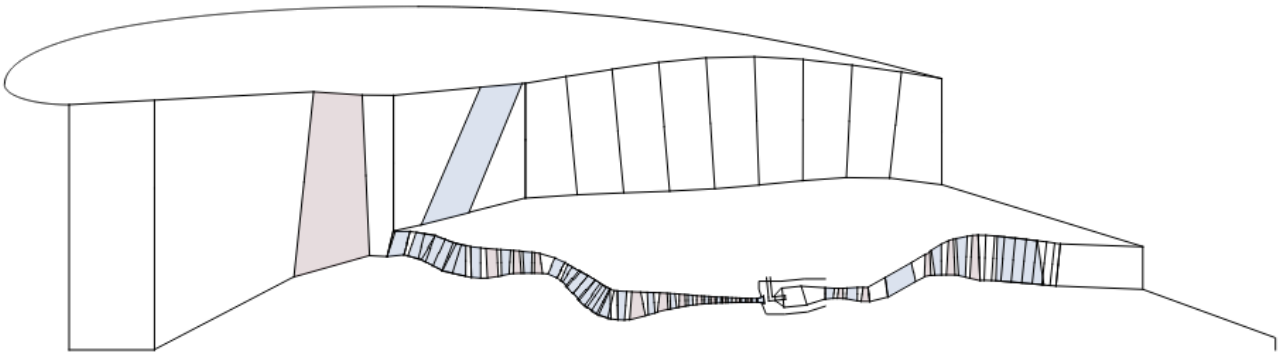

Figure 9 – Predicted two-dimensional annulus of the generic reference engine.

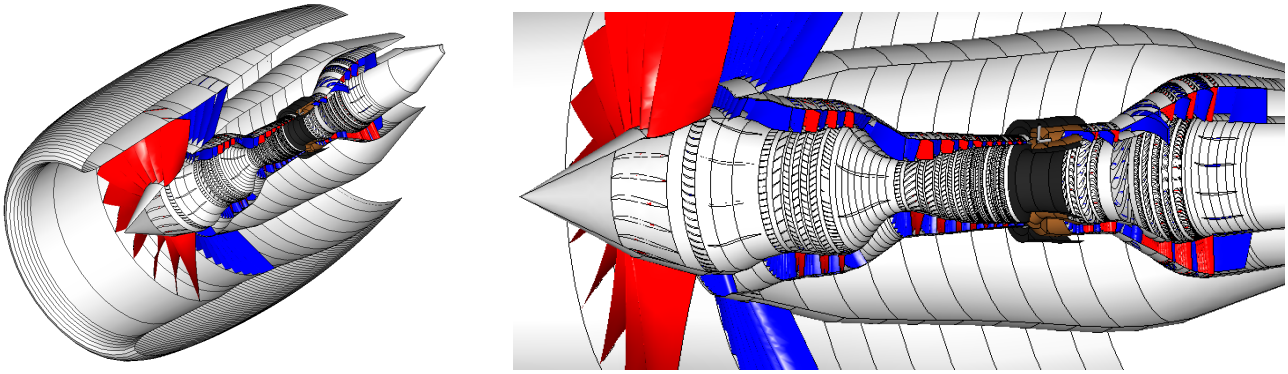

(a) Overall view (b) Core view

Figure 10 – 3D-view of the generic reference engine.

4.3 Mass Estimation

The mass breakdown for the generic engine using the component-based and part-based approach is presented in table 4. The prediction accounts only for the dry mass of the bare engine. The nacelle, thrust reverser and nozzles are not included. The gearbox mass is calculated with equation 38 for both approaches. Table 4 shows the total mass of the bare engine components and their relative share with respect to the total mass. The predicted bare engine mass of the generic engine is benchmarked with the reference: the PW1100G-JM weighs 2857.6 kg [43]. The generic engine model can only be compared to the PW1100G in terms of the bare engine mass since the masses of single components and parts are not available to the public domain.

4.3.1 Component-Based vs Part-Based Approach

The component-based procedure predicts 1847 kg and deviates from the reference mass by 35.4 %. The part-based approach results in a mass of 2887 kg and shows a deviation of 1.0 % compared to the reference. Please note, this close approximation is rather coincidence than the accuracy that can be expected for the part-based approach in general. Large deviations may occur on part level as will be discussed later in this section. However, more than one engine has to be calculated to deduce the accuracy of the method. According to Greitzer et al. [36, p. 138], the accuracy of WATE++ is in the order of $\pm$ 10 % with respect to the bare engine mass.

The comparison of masses on component level has to be done carefully considering equal or at least similar control volumes. In the following, both mass estimation methods are compared relative to each other. For both approaches the fan makes up the largest portion of the bare engine mass with $\approx$ 30 % but the predictions differ by 34.6 %. The predicted masses for the booster and HPC are similar for both methods with a difference of 19.5 and 22.1 %, respectively. The booster is lighter and the HPC is heavier in the case of the part-based method. The predicted combustor masses deviate by 21.7 % from each other but show a similar total mass share. The HPT is 19.8 % and the LPT 63.0 % heavier

Table 4 – Mass breakdown for the generic engine model.

Approach	Component-Based		Part-Based						
	Total	Share	Total	Share	Rotor	Stator	Disk	Connecting	Casing
Component	[kg]	[%]	[kg]	[%]	[%]	[%]	[%]	[%]	[%]
Fan	557	30.2	852	29.5	25.6	25.7	8.2	0.0	40.4
Fan Frame			191	6.6	-	-	-	-	-
ICD 1			31	1.1	-	-	-	-	-
Booster	104	5.6	87	3.0	9.1	20.7	24.9	2.6	42.6
ICD 2			19	0.7	-	-	-	-	-
Intermediate Frame			62	2.1	-	-	-	-	-
HPC	88	4.7	113	3.9	12.2	12.1	30.7	5.0	40.0
Combustor	54	2.9	69	2.4	-	-	-	-	-
HPT	89	4.8	111	3.8	3.3	18.2	51.3	1.3	25.9
ITD 1			13	0.4	-	-	-	-	-
LPT IGV Frame			52	1.8	-	-	-	-	-
LPT	227	12.3	370	12.8	12.5	15.1	39.0	1.1	32.2
TEC			66	2.3	-	-	-	-	-
TEC Frame			37	1.3	-	-	-	-	-
HP Shaft			9	0.3	-	-	-	-	-
LP Shaft			122	4.2	-	-	-	-	-
Gearbox	294	15.9	294	10.2	-	-	-	-	-
Accessories	233	12.6	389	13.5	-	-	-	-	-
Core Turbo Components	507	27.5	681	23.6	10.5	15.8	37.8	2.0	33.8
Turbo Components	1064	57.6	1532	53.1	18.9	21.3	21.4	0.9	37.5
Structure (Ducts, Frames, Shafts)	201	10.9	602	20.9	-	-	-	-	-
Bare Engine	1847	100.0	2887	100.0	10.0	11.3	11.4	0.5	19.9

in case of the part based approach. The total sum of core turbo components differ by 25.6 % and show similar shares with respect to the predicted bare engine mass.
The control volume for structural elements includes all shafts, ducts and frames. In the case of the component-based procedure, the structure is assumed to weigh 18 % (see Eq. 23) of the sum off all turbo components and the combustor which leads to 201 kg. With the part-based approach, the masses of single structural components are calculated taking into account their specific geometrical dimensions. In total, 602 kg are estimated for structure. Hence, the mass of structure is 3 times higher compared to the component-based approach.
For both approaches, a mass share of 15 % is assumed for accessories with respect to the sum of turbo components, structural components and the combustor. Therefore, the accessories mass is 40 % higher for the part-based approach due to heavier components.
In total, the part-based approach predicts a significantly higher bare engine mass compared to the component-based method. This difference is mainly caused by the estimates for the fan and structure. The component-based approach probably underestimates the structure mass since the prediction of the part-based approach is closer to the PW1100G-JM and the mass estimates of both methods for the core do not differ significantly. Hence, the component-based method according to Sagerser et al. [13] could be combined with the frame, shaft and duct models from [14, 15] to increase its accuracy while keeping the number of required input parameters for mass estimation limited. In the following sections, the part-based prediction is selected to be analyzed in detail due to the closer match of the reference mass and more available information on single parts.

4.3.2 Components on Engine Level

On the engine level, the turbo components have the largest mass fraction with 53.1 % according to the part-based approach (see Tab. 4). The second largest portion comes from the structural components with 20.9 % followed by the accessories, gearbox and combustor. Unfortunately, it is not possible to make a comparison with the component masses of the PW1100G-JM due to the lack of available data. But at least the plausibility of the predicted component masses can be verified by comparison with published studies. Donus et al. modeled the mass of six production engines and presented the

estimated relative mass shares of engine components and parts [19, p. 5]. There, the average relative deviation between the predictions and the component masses of the corresponding real engines is found to be between +17 and -22 %. The maximum deviation may be larger for each individual engine. Greitzer et al. modeled seven turbofan engines with WATE++ to deduce updated empirical coefficients for a more recent technological level based on information provided by Pratt & Witney and published the resulting mass breakdowns [36, p. 135-140].

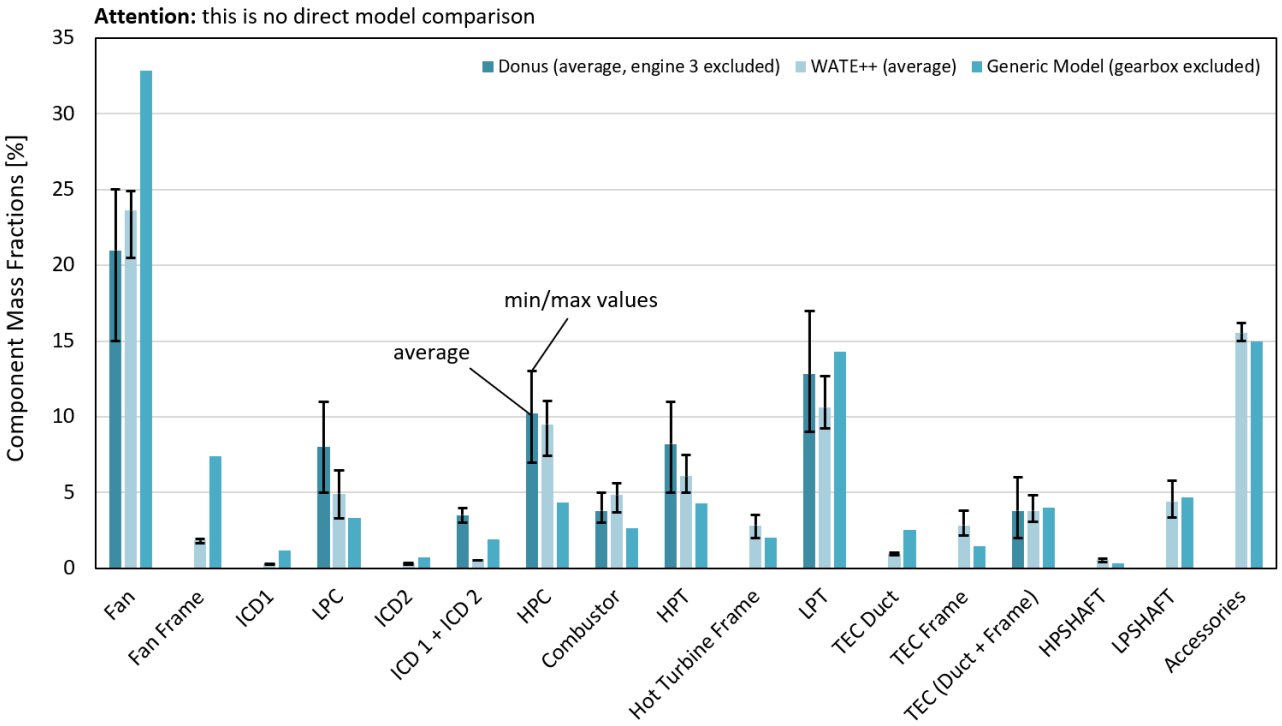

Figure 11 – Mass fraction of engine components with respect to the total bare engine mass: A comparison between averaged values for turbofan engines based on data from [19, 36] and the part-based predictions of the herein considered generic engine model. This is no direct model comparison but gives an indication of the validity of the calculated component masses.

The engines that belong to the published data differ from each other e.g. in size and thrust category, cycle parameters, engine architecture, number of stages and OEM. Hence, the relative mass fractions of components vary as well. For this work, the published breakdowns are averaged in order to derive approximate shares that are typical for turbofan engines. The data published by Donus et al. include a turboshaft engine (engine 3), which is excluded here because only turbofan engines are considered. In figure 11, the averaged data according to Donus et al. [19] and Greitzer et al. [36] is presented next to the estimated mass shares for the generic engine model. The error indicators show the minimum and maximum shares of the engine data from literature. The control volume for turbo components include rotors, stators, disks and connecting hardware e.g. disk wings. For the comparison, the gearbox was excluded from the bare engine mass of the generic model since the literature data only consist of conventional turbofans.

The fan mass fraction is higher for the generic engine compared to the literature data. One explanation for that is the engine bypass ratio. The average bypass ratio at sea level static of the WATE++ engines is 5.65 but the generic engine model has a value of up to 11. Thereby, the fan size increases relative to the core engine. This results in a larger mass fraction for the fan and favor smaller mass shares for core components. However, modern fans often have hollow blades and the blade volume factor K_v probably do not account for that. This could lead to an overestimation of the fan blade mass.

The fan frame is significantly heavier compared to the WATE++ data. Two shafts have to be supported due to the gearbox in case of the generic engine and the frame type 'Double-Bearing' was selected. Thus, an increase in the frame mass compared to conventional turbofan engines with the type 'Single-Bearing' is reasonable.

The mass share of the booster, HPC, combustor and HPT is smaller compared to the literature data. On the one hand this might be caused by smaller cores due to an increased bypass ratio. Furthermore, the generic engine model has an increased overall pressure ratio of 38 at sea level static in contrast to the WATE++ data with an average value of 32.3. This lead to a smaller size of the combustor, the HPT and the last HPC stages. Additionally, the number of stages in the compression section is lower compared to the WATE++ data. On the other hand the mass of the booster, HPC, combustor and HPT could be underestimated for the generic engine, e.g. due to the prediction of too light disks. Especially for the HPC, the predicted mass share is substantially below the minimum values of the reference data.
The mass share of the LPT is in agreement with the literature data. The LPT has to provide high power for the fan in the case of an increased bypass ratio. Therefore, the exhaust gas has to be expanded to a low pressure level which leads to increased size in the rear part of the turbine. In addition, the LPT of the generic engine model is fast-running due to the gear. Therefore, heavier disks and casings have to be expected. In contrast, only three stages in case of the generic model compared to 4 to 7 stages in the WATE++ data indicates a smaller mass fraction for the LPT.
The mass fractions of remaining frames, ducts and shafts show good agreement with the literature data. Masses for the compresser intermediate case (ICD2) and the TEC of the PW1100G series can be found in [44]. According to the size of the generic model, the intermediate case has a mass of 70 kg and 81 kg are predicted by the part-based approach (duct and frame). For the TEC a mass of 75 kg is published and 103 kg are predicted. Hence, the estimated values are good approximations but with a deviation of 15.7 and 37.3 % too heavy.
In summary, the estimated component mass shares for the generic model seem justifiable although there is an uncertainty for core components. The mass of modern structural components could be overestimated by the prediction method as it is indicated for the intermediate and turbine exhaust case.

4.3.3 Parts on Component Level

The portion of rotors, stators, disks, connecting hardware and casing with respect to the corresponding component mass is shown for the part-based approach in table 4.

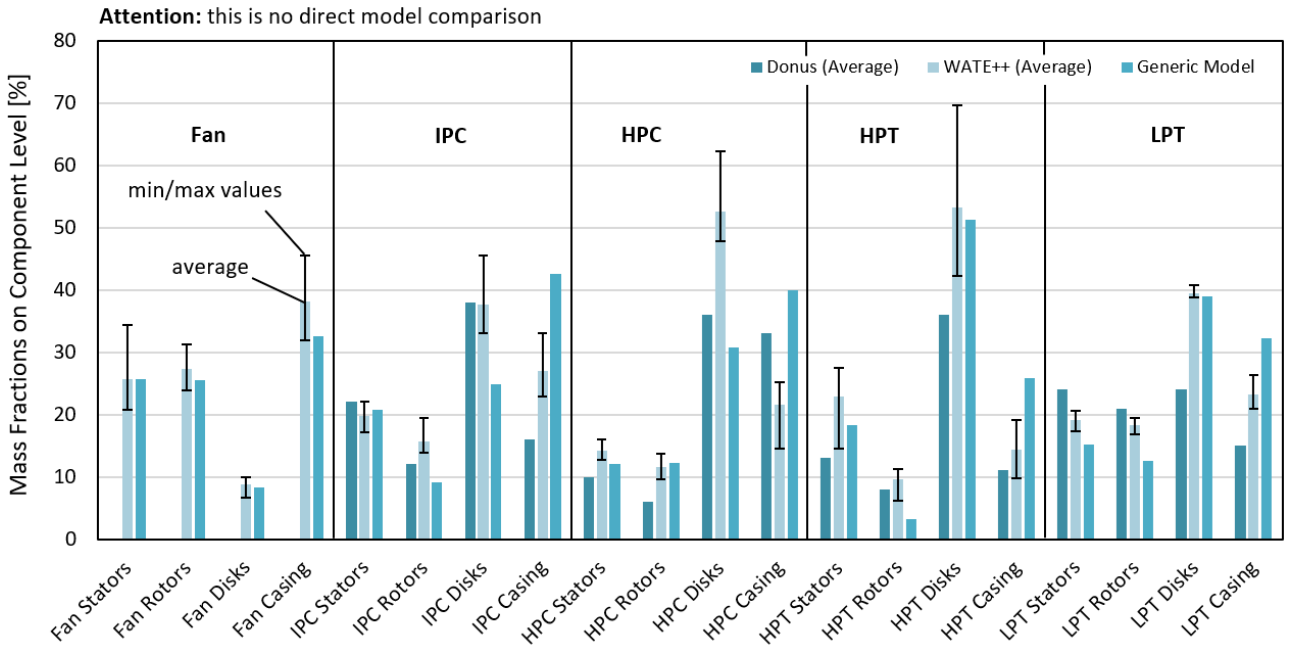

Figure 12 – Mass fraction of parts with respect to the total component mass: A comparison between averaged values for turbofan engines based on data from [19, 36] and the part-based predictions of the herein considered generic engine model. This is no direct model comparison but gives an indication of the validity of the calculated part masses.

The fan is dominated by its casing, followed by the blades and the disk, which has only a small share. The relative mass fraction of disks increases for the core compressors and makes up the highest fraction in case of the turbines. The casing contributes substantially to the masses of compressors and turbines in the core with a relative mass share of 40.0 to 42.6 % and 25.9 to 32.2 %, respectively. Thus, disks and casings are the heaviest parts on the core engine level. But on the overall engine level where the fan is included, rotors, stators and disks have a similar mass fraction with ≈ 10-12 % (see Tab. 4). The major contributors to the bare engine mass are structural components, blades and the casing with ≈ 20 % for each.
In the following, the plausibility of the part estimates on component level is analyzed. The relative share of parts on component level is shown in figure 12 comparing the data from Donus et al. and Greitzer et al. (WATE++ surrogate model) to the part-based predictions for the generic engine model. This is no direct model comparison for the same boundary conditions but it can be checked if the herein applied methods lead to predictions that deviate from typical mass distributions of turbofan engines.
The mass distribution for the fan matches well with the WATE++ data. For the booster (IPC) and the HPC, the comparison indicates too light disks and a too heavy case for the generic model. The mass shares of the blades seem to be plausible for all compressors. The relative mass shares of turbine casings are predicted with higher values compared to the literature data. In addition, lower mass fractions are observed in case of turbine rotor blades.
The calculated casing thickness for turbo components is presented in table 5. The model for the rotor containment thickness of the fan was calibrated to match the approximated value from the drawing of the PW1100G. For the other components, the thicknesses are calculated with $C_{case} = 1.0$. The thickness for the booster and HPC seem to be in a plausible order of magnitude. But for the HPT and LPT, values similar to the fan rotor containment are calculated which is probably too thick. Therefore, the impact of the turbine casing on the component mass is probably overestimated. This could explain the large mass fractions of the casing that are observed.

Table 5 – Calculated average casing thickness for turbo components.

	Unit	Fan Rotor	Booster	HPC	HPT	LPT
t_{case}	*[mm]*	13.6	8.41	7.1	13.1	14.4

4.3.4 Mass Prediction for Disks

In order to asses the accuracy of the disk mass calculation, disk volumes are roughly approximated from the scaled engine drawing published in [41]. The fan disk is predicted well with a deviation of -16 %. For the core engine, the predicted disk volume is constantly underestimated. Mean deviations of -31 %, -42 % and -20 % are achieved for the booster, HPC and HPT, respectively. For these components, the maximum deviation occurs at the last HPC stage with -59 %. The underestimation of compressor disks is in agreement with the observations from section 4.3.3. In case of the LPT, the predicted volume of the last disk is with +108 % significantly overestimated. The rotor blades of the last LPT stage of the PW1100G are made of titanium-aluminid (TiAl). With this material the blade density [45] and blade mass [46] decrease approximately to the half. Hence, the required disk thickness is reduced as well. But for the generic model, all blades are calculated with the material properties of nickel-based alloys. This explains the large deviation for the last LPT stage. In total, the LPT has an average deviation of 25 % compared to the approximated values from the drawing. The sum off all disks deviates by -11 %.
The correlation accuracy of ± 30 % stated by Klees et al. [15, p. 11] can not be confirmed for single disks of a modern geared turbofan engine. But due to the clear trend of underestimation except for the LPT, the correlation may be re-calibrated to eliminate the off-set and to improve its accuracy for the latest generations of engines. With the extracted disk volumes, the relative disk thickness can be calculated and compared to the correlations of Klees et al. [15] that are introduced in section 3.2.2. To account for the different materials, the relative disk load is multiplied by the ratio of yield strengths before it is plotted in figure 13. The data point for the third disk of the LPT is excluded since

the blades are made of TiAl. The data points show a comparable trend as the correlation for steel compressor and turbine disks that was applied to calculate the generic engine model. Furthermore, the data points correlate well with the relative disk load $\sigma_{disk,rel}$ and a new correlation is deduced. The new disk correlation fits better for the validation case especially for low disk loads.

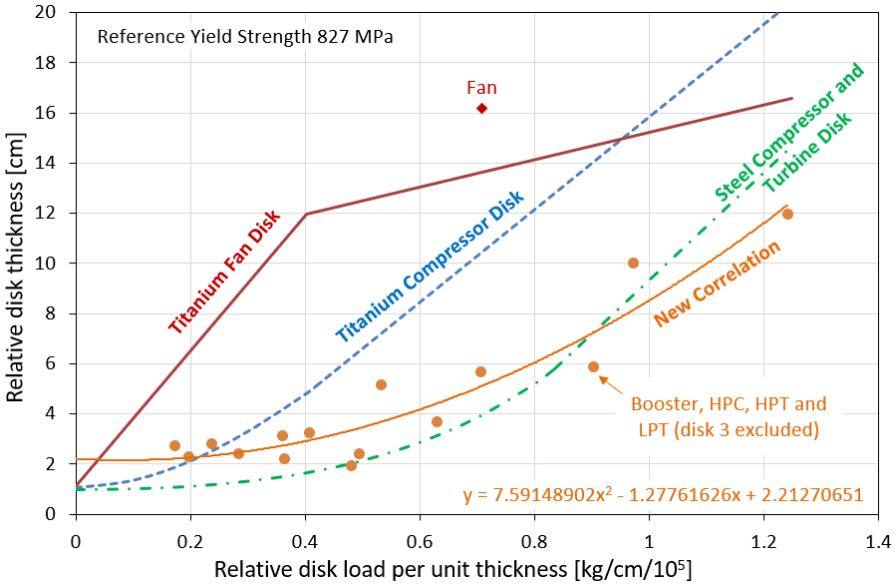

Figure 13 – Disk thickness correlations according to [15] extended by the new correlation that was deduced for the validation case.

5. Trend Analysis

During an MDAO process, a redesign of the engine becomes necessary due to changed boundary conditions such as the thrust requirement or maximum permissible engine diameter. Furthermore, engine design parameters are varied to find the optimal design on the overall aircraft level. In the following, a design study is performed in order to investigate the capability of the geometry and mass process to adapt to variations.

5.1 Design Rules

Different design laws are applied to ensure feasible engine designs. The flight conditions, the thrust demand[1] and the engine off-takes remain the same for the considered operating points. Constant polytropic efficiencies of turbo components are prescribed for cruise and generic component maps are evaluated for other operating conditions. A correction of the turbo component efficiencies is applied to account for Reynolds number effects at different flight altitudes similar to [47, p. 167]. The cooling air demand for the HPT stages is estimated at the maximum take-off condition using a model similar to [47, p. 248] and considering the temperatures T_3 and T_{41}. The rotational speed of the HP and LP shaft is determined by matching maximum values for the mean circumferential blade velocity at the inlet of the HPC and the outlet of the LPT, respectively. The gear ratio of the power gearbox is selected by matching the reduced circumferential velocity at the fan tip that is modeled in dependence on the fan pressure ratio according to [47, p. 174]. The pressure split between the booster and HPC is held constant. The maximum temperature limits for T_3 and T_{41} are also held constant[2] (see Tab. 1). The fan pressure ratio is selected to achieve the optimal ratio of nozzle velocities for an unmixed turbofan engine. The input parameters for geometry and mass estimation that are shown in table 2 from section 4.1 are not changed during the study. The only exception is the fan inlet Mach number. The fan inlet Mach number is selected by matching a maximum value for the flow capacity of the fan that is reached at one of the considered operating conditions (see Tab. 1). The stage count for the booster, HPC and

[1] Except for the thrust variation where the thrust ratios between the operating conditions are held constant.
[2] With the exception of the OPR or T_{41} variation that will be conducted

LPT is estimated based on a maximum allowed stage loading coefficient $\psi_{max,stage}$ at cruise conditions (see step 9 in Sec. 3.1.2). The stage numbers of the fan and HPT are kept constant. This set of design rules accounts for relevant thermodynamic interdependencies and constraints during the conceptual engine design but there are limitations since not all effects are captured. For example, the influence of size and loading on the efficiency of turbo components is currently not considered.

5.2 Calibration and Trend Validation

In order to validate the generated trends for the bare engine mass and length, a comparison with the surrogate model for 'correlation-based' predictions published in [36, p. 143-145] is made. This surrogate is based on WATE++ calculations and was created to cover a broad range of geared turbofan engines with different bypass ratios, overall pressure ratios and mass flows. To compare the trends of mass and length, the component-based and part-based approach as well as the predictions from the WATE++ surrogate model are calibrated. Therefore, calibration factors C_i are introduced in the form

$$X_{i,calibrated} = C_i \, X_i \tag{39}$$

The calibration factors are determined by matching the mass of the PW1100G-JM and the same length when they are evaluated for the generic reference engine that was used for calibration (see Sec. 4.). In table 6, the mass and length predictions with the corresponding calibration factors are listed. The bare engine length is measured from the spinner to the TEC flange. In contrast to the PW1100G, here the spinner is modeled as a linear cone. The WATE++ surrogate model predicts a bare engine mass of 2062 kg and underestimates the reference mass by 27.8 %. The exact definition of engine length for the WATE++ model is not specified in [36] but the prediction is significantly smaller than the reference length. By applying the calibration factors all models estimate the same values for the generic reference engine from section 4.

Table 6 – Bare engine mass and length predictions for the generic reference and calibration factors.

Parameter	unit	Component-Based	Part-Based	WATE++ surrogate
Bare engine mass	[kg]	1847	2887	2062
$C_{mass,i}$	[-]	1.548	0.990	1.386
Bare engine length	[m]	3.613	3.613	2.175
$C_{length,i}$	[-]	1.0	1.0	1.661

The calibration procedure scales all masses by the same factor. When a model underestimates e.g. the fan mass but makes good predictions for all other components, not only the trend for the fan but also the 'correct' trend of other components is scaled. This may lead to prediction errors for design variations. Without calibration, the part-based approach predicts the mass of the reference engine with the smallest deviation with respect to the PW1100G-JM and has therefore a calibration factor close to 1 eliminating this source of error.

5.3 Variation of Engine Design Parameters

The bypass ratio (BPR), required thrust, overall pressure ratio (OPR) and stator outlet temperature of the HPT (T_{41}) are varied starting from the generic reference turbofan. Only one design parameter is varied at once and a new engine is designed for each parameter value with respect to the described design rules. It is examined whether physically reasonable geometry and mass estimates of the overall engine can be achieved. Besides the trends on overall engine level, the masses of individual components that are predicted with the part-based approach are presented.

Bypass Ratio

The trends that result from a variation of the engine bypass ratio are shown in figure 14. With an increasing BPR, the fan pressure ratio $\pi_{Fan,Byp}$ and the jet velocities decrease. This leads to an

improved propulsive efficiency and TSFC but also to higher mass flows and a larger fan diameter. The number of required HPC stages reduces by one at low BPRs since the fan has an elevated pressure ratio in this region and the HPC compresses the fluid less until the T_3-limit is reached. The bare engine mass and length increase steadily with BPR and the three calibrated models for mass estimation predict almost the same trend. The largest difference in the predicted mass occur at low BPR with maximum 5 % between the part-based method and the WATE++ surrogate model. The estimated geometry of the engine with the largest investigated BPR is depicted in comparison to the generic reference engine in figure 15. The additional length comes primarily from the fan.

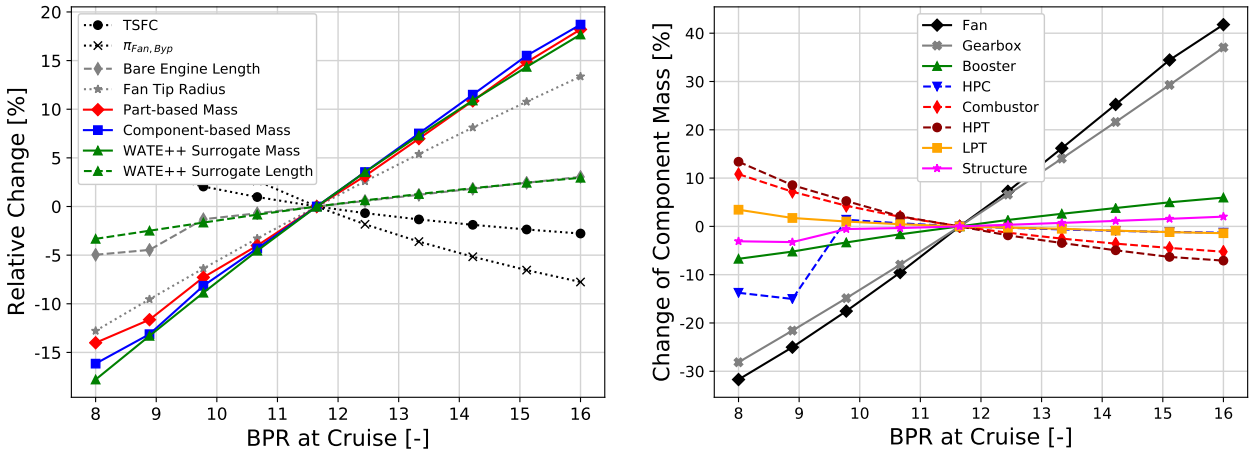

(a) Overall engine parameters

(b) Part-based predictions on component level

Figure 14 – Variation of the engine bypass ratio.

In figure 14b, the relative change of component masses is depicted. The increase in the total bare engine mass with the BPR is mainly driven by the fan and gearbox. The fan size increases significantly relative to the core engine while the mass of the hot section is reduced. The size and mass of the booster grow slightly with the BPR since the pressure ratio over the fan is reduced and the fluid has a higher volume flow at the core inlet.

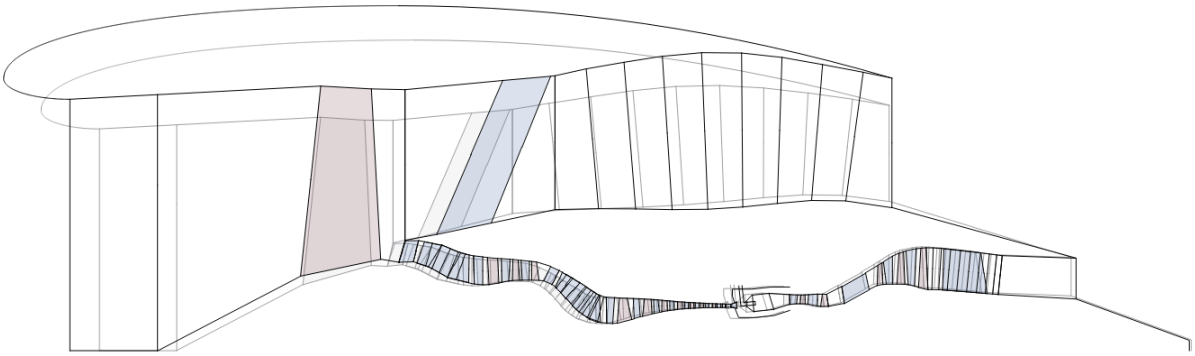

Figure 15 – Engine geometry for the highest investigated bypass ratio in direct comparison to the generic reference (shaded).

Thrust

A variation of the engine thrust while maintaining the thrust ratios between the sizing operating points leads to the figures 16 and 17. The TSFC and fan pressure ratio change marginal since the assumed absolute values for power off-takes and customer bleed remain the same. The mass, length and fan radius increase almost linear due to higher engine mass flows that are required to fulfill an increasing thrust demand. Nonlinear variations have to expected when the thrust ratios between the sizing

operating points are changed. A difference in the slope is observed for the bare engine mass when the mass estimation models are compared. The predicted masses of the component-based and part-based method are relatively close together which is reasonable since they are based on the same geometrical model. Similar trends are also found when the approach of this paper is compared to the WATE++ surrogate model. The maximum deviation of 10 % in mass occurs at high thrust between the part-based model and the WATE++ surrogate for which the WATE++ geometry model was used. The same trend can be observed for the engine length.

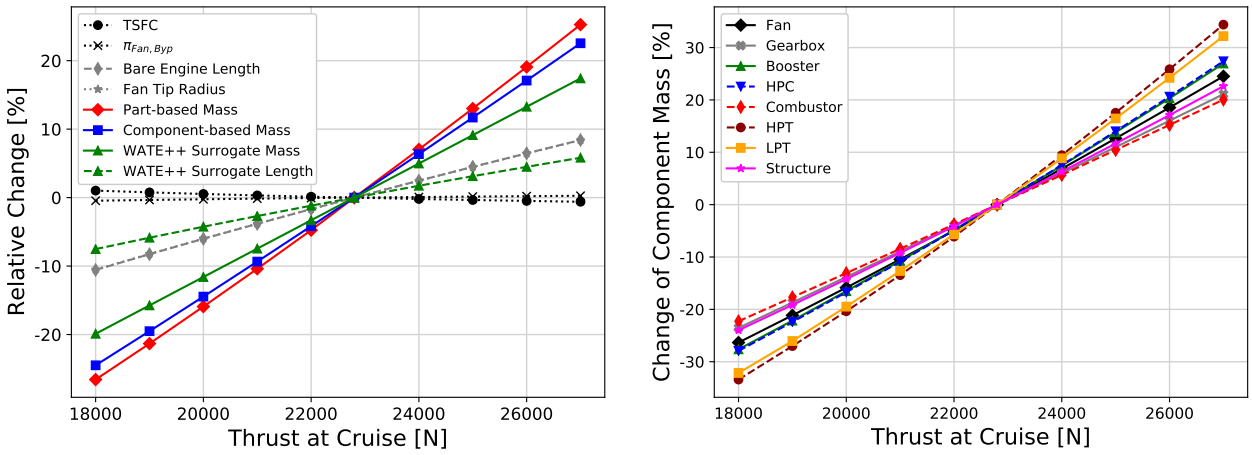

(a) Overall engine parameters

(b) Part-based predictions on component level

Figure 16 – Variation of engine thrust.

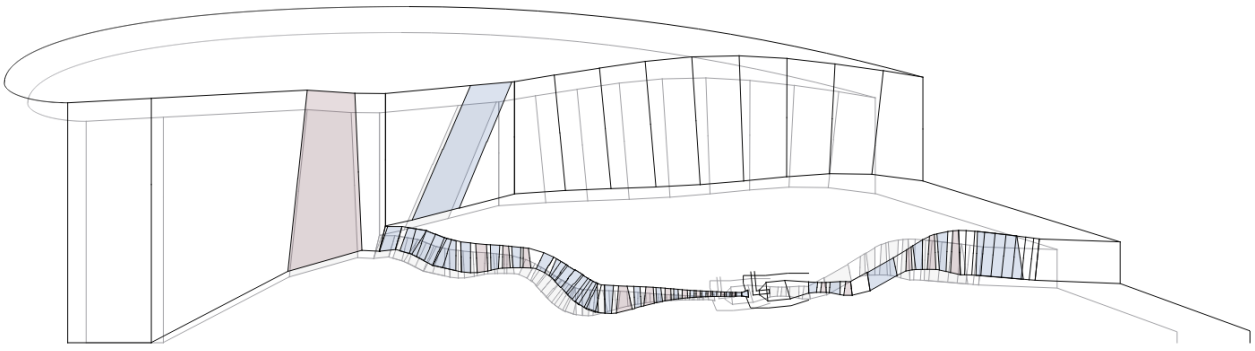

Figure 17 – Engine geometry for the highest investigated thrust in direct comparison to the generic reference (shaded).

Overall Pressure Ratio

A variation of the OPR is shown in figure 18 and the geometry of the engine with the highest investigated OPR is depicted in direct comparison to the reference model in figure 19. The pressure ratio of the fan follows a contrary trend as the OPR. After the extraction of the required power to drive the compressors, less residual energy is available in the exhaust gas at a higher OPR. Hence, the jet velocities of the core and bypass decrease maintaining the optimal velocity ratio. This velocity reduction leads to a lower pressure ratio of the fan. In addition, with a growing OPR and combustor inlet temperature T_3, the heat or more specifically the fuel flow that can be added until the maximum allowable turbine temperature limit is reached shrinks. Both effects result in a demand for higher mass flows to meet the required thrust. Therefore, the fan diameter, engine mass and length grow with the OPR (see Fig. 16a). The TSFC first improves with an increasing OPR because of a growing thermal and propulsive efficiency, reaches a minimum and then gets worse partially due to a growing cooling

air demand. To keep the loading below the limit $\psi_{max,stage}$, discrete steps in the required stage count of the HPC can be observed when OPR increases. This leads to discrete steps in bare engine mass and length. The trend of the engine length is in good agreement with the WATE++ surrogate that cannot capture discrete steps. The mass estimation methods show similar trends but maximum deviations in the order of 3 %.

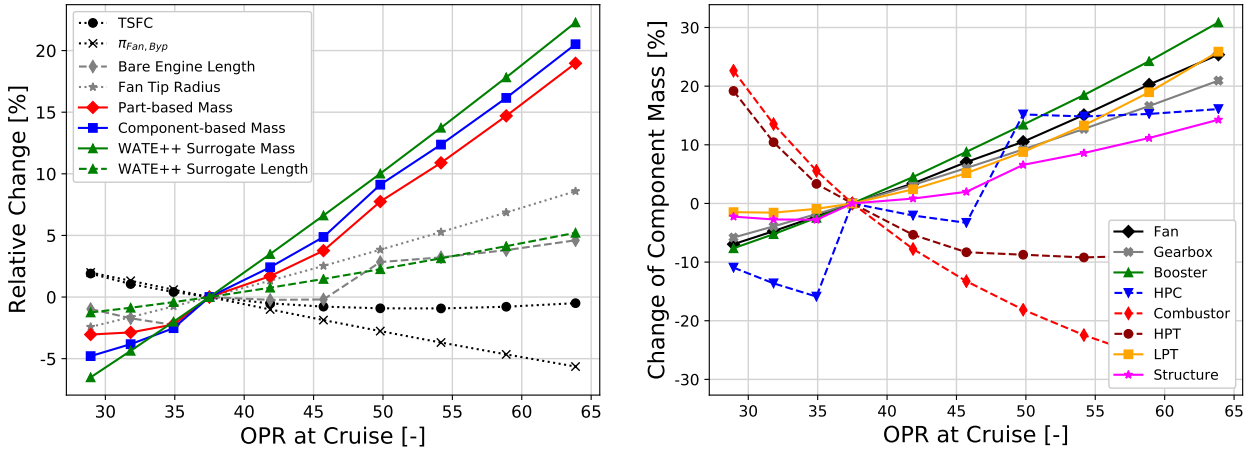

(a) Overall engine parameters

(b) Part-based predictions on component level

Figure 18 – Variation of the overall pressure ratio.

The relative mass change of the engine components shows contradictory trends (see Fig. 18b). The HPC mass makes discrete steps when an additional stage is added and decreases in between. The combustor and HPT also show a mass reduction with increasing OPR due to the higher pressure level and smaller component dimensions (see Fig. 19). The mass of other engine components increase because of the growing mass flow demand and the related component size. The booster shows the largest relative mass gain. Not only the mass flow through the booster increases but also the inlet pressure and density decreases with the fan pressure ratio which contribute to a high volume flow.

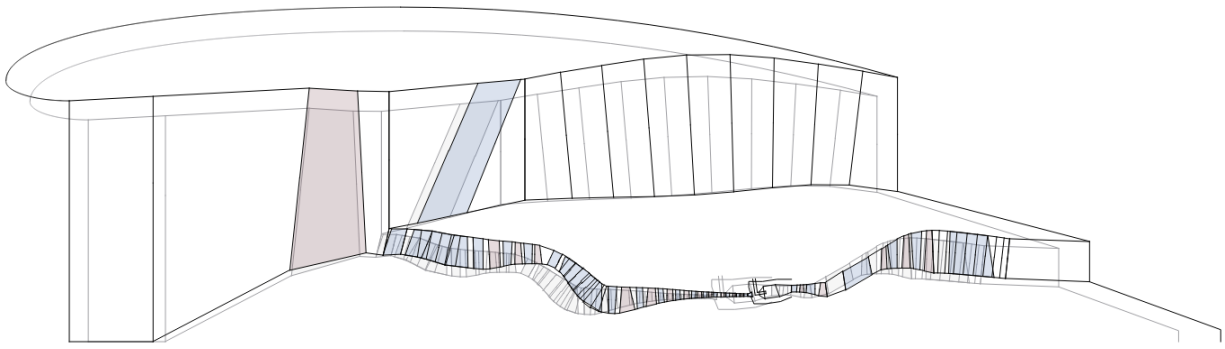

Figure 19 – Engine geometry for the highest investigated overall pressure ratio in direct comparison to the generic reference (shaded).

Turbine Temperature

A variation of the stator outlet temperature of the first HPT stage T_{41} at cruise is presented in figure 20. The temperature level is elevated with T_{41} not only for cruise but for all considered operating points. An increase in T_{41} allows to add and burn more fuel per core mass flow. Hence, the power density of the core engine grows and the core mass flow can be reduced for a constant thrust demand. Furthermore, the residual energy of the exhaust gas after the expansion in the turbine section increases with T_{41} for a constant OPR. This leads to higher jet velocities for both nozzles and makes a larger fan pressure

ratio necessary whereby the required engine mass flow shrinks further to match the prescribed thrust. This mass flow reduction leads to smaller engine dimensions as can be observed in figure 21 that compares the engine with the highest investigated temperature to the generic reference case. In figure 20a, the corresponding decreasing trend of engine length and fan radius with higher temperatures becomes clear. The bare engine mass is also reduced due to the smaller engine dimensions and all engine components show a clear decreasing trend with different slopes (see Fig. 20b). The strongest relative mass reduction occurs for the HPT. In addition to the smaller core mass flow, the inlet area further reduces due to an elevated level of temperature and speed of sound at the inlet while a constant Mach number is assumed.

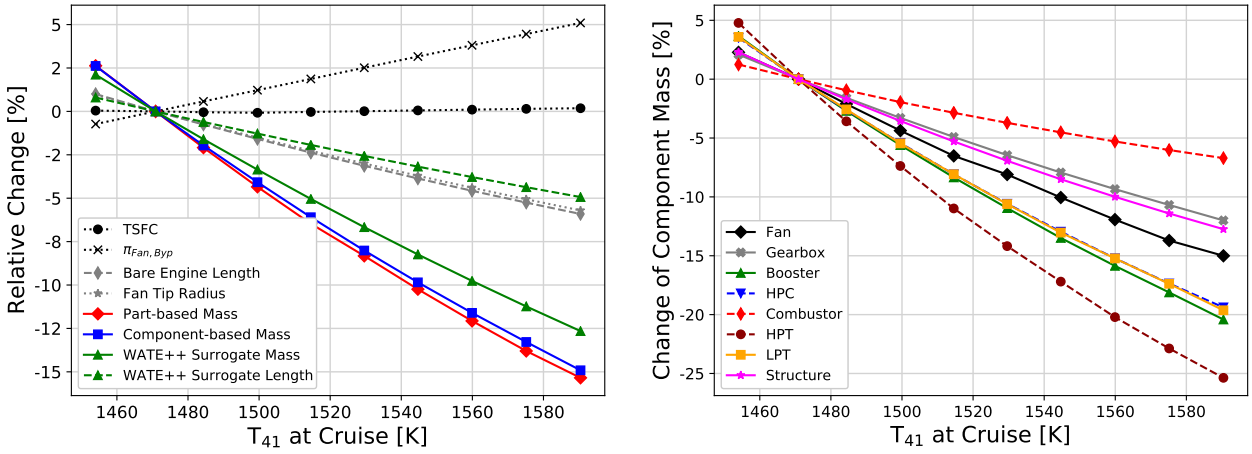

(a) Overall engine parameters

(b) Part-based predictions on component level

Figure 20 – Variation of the stator outlet temperature T_{41}.

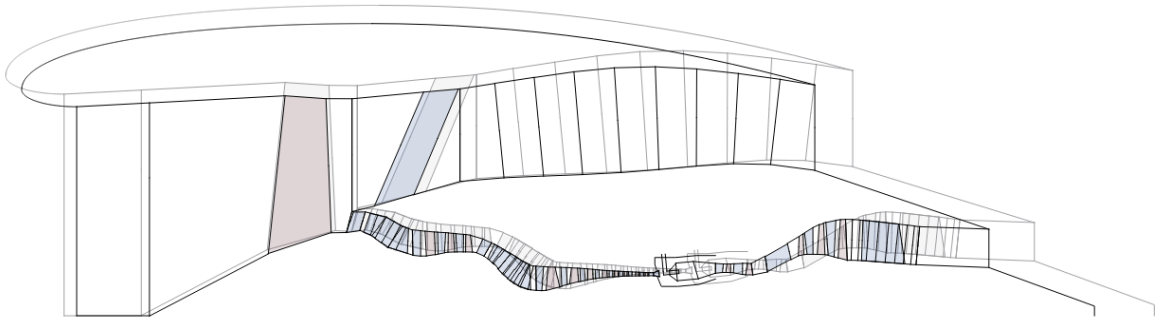

Figure 21 – Engine geometry for the highest investigated turbine temperature in direct comparison to the generic reference (shaded).

5.4 Discussion

The conducted parameter variations produce reasonable trends and show that the presented estimation approach accounts for interdependencies between the thermodynamic cycle, engine geometry and mass. It became clear that the engine mass flow has a significant influence on both size and mass but does not only scale with thrust. At a first glance, it seems trivial to estimate this mass flow using thermodynamic cycle analysis. In order to derive a feasible engine model during conceptual design, a carefully selected set of design rules has to be applied taking into account all sizing operating conditions. Furthermore, it is mandatory to consider the design limitations of and interdependencies between the individual components. The selected design laws that are used for the presented study attempt to meet this challenge. However, several effects are not considered e.g. the influence of size

and loading on the efficiency of turbo components. The component-based and part-based results are in good agreement since the same thermodynamic and geometrical model is used for mass estimation and both approaches are calibrated with respect to the reference engine. The calibrated WATE++ surrogate model shows trends for the bare engine mass and length that are in good agreement with the model that is developed in this paper. This is partly caused by the same underlying thermodynamic model that is used for mass prediction but also verifies the correctness of the implemented mass estimation procedure herein. Deviations may be related to different assumptions for input parameters e.g. K_v, differences in the methodology e.g. disk mass calculation or regularization errors during the fitting process of the WATE++ surrogate model e.g. caused by discrete steps in stage count [36, p. 144-145]. Furthermore, the surrogate model capture changes in the turbine temperature and thrust only through the core reduced mass flow at take-off.

6. Conclusion

A knowledge-based approach for the estimation of engine geometry during conceptual design was presented. The approach makes use of B-splines and enables the prediction of turbo components with complex annulus shapes based on a few input parameters during design studies. Sufficient details have been provided to allow the implementation for the reader.

For mass estimation, a component-based and a part-based method were benchmarked for a generic geared turbofan that was used as a validation case and is similar to the PW1100G. The results are compared to available data from the literature to verify the plausibility of calculated masses. In order to investigate one source of uncertainty that was found, the disk mass predictions are analyzed in detail and an improved disk correlation was derived based on the validation case.

With the conducted parameter studies, it was demonstrated that the implemented approach is capable of predicting plausible trends by accounting for interdependencies between thermodynamics, geometry and mass. The applied component-based, part-based and correlation-based models produce similar trends after calibration.

The authors recommend the correlation-based method (WATE++ surrogate model) according to Greitzer et al. to make initial predictions for overall aircraft design where the focus lays on the aircraft and not on the engine. But in order to achieve feasible mass trends, the importance of high-quality data on the thermodynamic cycle which is typically provided by engine performance engineers should not be undervalued. For MDAO studies or when the engines move more in the focus, the herein described approach for geometry generation is recommend combined with the part-based approach for mass estimation. This combination of methods enables the holistic assessment of design variations on engine level and the provision of performance, geometry and mass data to create rubber engine models for an overall aircraft MDAO.

7. Contact Author Email Address

Jannik Häßy
German Aerospace Center (DLR)
Institute of Propulsion Technology
Cologne, Germany
mailto: Jannik.Haessy@dlr.de

8. Copyright Statement

References

[1] D. P. Raymer, *Aircraft design, A conceptual approach* (AIAA Education Series), eng, 2. print. Washington: American Inst. of Aeronautics and Astronautics, 1989, 729 pp., ISBN: 0-930403-51-7.

[2] J. J. Berton and M. D. Guynn, "Multi-objective optimization of a turbofan for an advanced, single-aisle transport," *Journal of Aircraft*, vol. 48, no. 5, pp. 1795–1805, 2011, ISSN: 0021-8669. DOI: 10.2514/1.C031333.

[3] M. Drela, *Simultaneous optimization of the airframe, powerplant, and operation of transport aircraft*, M. Drela, Ed., MIT Department of Aeronautics and Astronautics, 2010. [Online]. Available: http://web.mit.edu/drela/Public/papers/RAeS/rt.pdf.

[4] A. Seitz, "Advanced methods for propulsion system integration in aircraft conceptual design," Dissertation, Technische Universität München, München, 2012, 205 pp.

[5] W. Lammen, P. Kupijai, D. Kickenweitz, and T. Laudan, "Integrate engine manufacturer's knowledge into the preliminary aircraft sizing process," *Aircraft Engineering and Aerospace Technology*, vol. 86, no. 4, pp. 336–344, 2014, Richard Degenhardt, Dr Leslie J. Co, Prof (Editor), ISSN: 0002-2667. DOI: 10.1108/AEAT-10-2012-0190.

[6] P. Kupijai, *Ein Beitrag zur automatisierten Triebwerksvorauslegung*, Zugl.: Cottbus-Senftenberg, Techn. Univ., Diss., 2014 (Berichte aus der Luft- und Raumfahrttechnik), ger. Aachen: Shaker, 2014, 182 pp., ISBN: 9783844028386.

[7] J. Häßy, J. Schmeink, R. Becker, S. Reitenbach, M. Vieweg, P. Bekemeyer, and A. Merle, "Hybrid surrogate-based rubber engine model for aircraft multidisciplinary design optimization," in *AIAA AVIATION 2020 FORUM*, (VIRTUAL EVENT), Reston, Virginia: American Institute of Aeronautics and Astronautics, 6152020, ISBN: 978-1-62410-598-2. DOI: 10.2514/6.2020-3186.

[8] S. Reitenbach, C. Hollmann, J. Schmeink, M. Vieweg, T. Otten, J. Haessy, and M. Siggel, "Parametric datamodel for collaborative preliminary aircraft engine design," in *AIAA Scitech 2021 Forum*, (VIRTUAL EVENT), Reston, Virginia: American Institute of Aeronautics and Astronautics, 1112021, ISBN: 978-1-62410-609-5. DOI: 10.2514/6.2021-1419.

[9] R.-G. Becker, S. Reitenbach, C. Klein, T. Otten, M. Nauroz, and M. Siggel, "An integrated method for propulsion system conceptual design," in *Proceedings of the ASME Turbo Expo: Turbine Technical Conference and Exposition - 2015, Presented at the ASME 2015 Turbo Expo: Turbine Technical Conference and Exposition, June 15 - 19, 2015, Montreal, Quebec, Canada*, (Montreal, Quebec, Canada,), American Society of Mechanical Engineers and International Gas Turbine Institute, New York, NY: ASME, 2015, ISBN: 978-0-7918-5662-8. DOI: 10.1115/GT2015-43251.

[10] S. Reitenbach, A. Krumme, T. Behrendt, M. Schnös, T. Schmidt, S. Hönig, R. Mischke, and E. Mörland, "Design and application of a multidisciplinary predesign process for novel engine concepts," *Journal of Engineering for Gas Turbines and Power*, vol. 141, no. 1, 2019, ISSN: 0742-4795. DOI: 10.1115/1.4040750.

[11] S. Reitenbach, M. Vieweg, R. Becker, C. Hollmann, F. Wolters, J. Schmeink, T. Otten, and M. Siggel, "Collaborative aircraft engine preliminary design using a virtual engine platform, part a: Architecture and methodology," in *AIAA Scitech 2020 Forum*, (Orlando, FL), Reston, Virginia: American Institute of Aeronautics and Astronautics, 1062020, ISBN: 978-1-62410-595-1. DOI: 10.2514/6.2020-0867.

[12] J. Schmeink, A. Görtz, and J. Häßy, "Application of a global sensitivity screening method for design space exploration of coupled turbofan engine performance and preliminary design," in *Proceedings of Global Power and Propulsion Society GPPS 2020*. DOI: 10.33737/gpps20-tc-71.

[13] D. A. Sagerser, S. Lieblein, and R. P. Krebs, *Empirical expressions for estimating length and weight of axial-flow components of vtol powerplants*, NASA, 1971.

[14] R. J. Pera, E. Onat, G. W. Klees, and E. Tjonneland, *A method to estimate weight and dimensions of aircraft gas turbine engines, Volume i: Method of analysis*, NASA, 1977.

[15] G. W. Klees and L. H. Fishbach, "Aircraft engine weight estimation method," in *Thirty-Seventh Annual Conference*, (Munich, West Germany), Society of Allied Weight Engineers, Inc., Ed., Society of Allied Weight Engineers, Inc., 1978.

[16] M. T. Tong and B. A. Naylor, "An object-oriented computer code for aircraft engine weight estimation," in *Proceedings of the ASME Turbo Expo 2008, Presented at the 2008 ASME Turbo Expo, June 9 - 13, 2008, Berlin, Germany*, (Berlin, Germany,), American Society of Mechanical Engineers and International Gas Turbine Institute, New York, NY: ASME, 2008, pp. 1–7, ISBN: 978-0-7918-4311-6. DOI: 10.1115/GT2008-50062.

[17] P. Lolis, "Development of a preliminary weight estimation method for advanced turbofan engines," School of Engineering, Department of Power and Propulsion, Dissertation, Cranfield University, 2014.

[18] R. Schaber, "Numerische auslegung und simulation von gasturbinen," Fakultät für Maschinenwesen, Dissertation, Technische Universität München, 2000, 115 pp.

[19] F. Donus, R. Schaber, K.-J. Schmidt, and S. Staudacher, "Accuracy of analytical engine weight estimation during the conceptual design phase," in *Proceedings of the ASME Turbo Expo 2010, Presented at the 2010 ASME Turbo Expo, June 14 - 18, 2010, Glasgow, UK*, (Glasgow, UK,), American Society of Mechanical Engineers and International Gas Turbine Institute, New York, NY: ASME, 2010, pp. 1377–1384, ISBN: 978-0-7918-4401-4. DOI: 10.1115/GT2010-23774.

[20] S. Bretschneider, "Knowledge-based preliminary design of aero-engine gas-generators," Institut für Luftfahrtantriebe, Dissertation, Universität Stuttgart, Stuttgart, 2011. [Online]. Available: dissertation.de.

[21] A. Keskin, *Process integration and automated multi-objective optimization supporting aerodynamic compressor design*, Zugl.: Cottbus, Techn. Univ., Diss., 2006 (Berichte aus der Luft- und Raumfahrttechnik), eng. Aachen: Shaker, 2007, 138 pp., ISBN: 3832258752.

[22] M. Hinz, "Neue parametrisierungsstrategien und methoden der prozessbeschleunigung für die verdichteroptimierung," Fakultät für Maschinenbau, Elektrotechnik und Wirtschaftsingenieurwesen, Dissertation, Brandenburgischen Technischen Universität Cottbus, Cottbus, 2012, 180 pp.

[23] P. Lolis, P. Giannakakis, V. Sethi, A. J. B. Jackson, and P. Pilidis, "Evaluation of aero gas turbine preliminary weight estimation methods," *The Aeronautical Journal*, vol. 118, no. 1204, pp. 625–641, 2014, PII: S0001924000009404, ISSN: 0001-9240. DOI: 10.1017/S0001924000009404.

[24] L. T. Whitehead and J. Brown, *A mechanical design for a lightweight turbo-jet engine and the variation of engine weight with size*, National Gas Turbine Establishment, 1953.

[25] W. A. Pennington, "Choice of engines for aircraft," *Shell Aviation News*, no. January 1959, pp. 14–19, 1959.

[26] R. P. GEREND and J. P. ROUNDHILL, "Correlation of gas turbine engine weights and dimensions," in *6th Propulsion Joint Specialist Conference*, (San Diego,CA,U.S.A), Reston, Virigina: American Institute of Aeronautics and Astronautics, 1970. DOI: 10.2514/6.1970-669.

[27] E. Torenbeek, *Synthesis of subsonic airplane design, An introd. to the preliminary design of subsonic general aviation and transport aircraft, with emphasis on layout, aerodynamic design, propulsion and performance*, eng, [Student ed.] Delft and The Hague: Univ. Pr and Nijhoff, 1982, 598 pp., ISBN: 90-247-2724-3.

[28] V. Sanghi, S. K. Kumar, V. Sundararajan, and S. K. Sane, "Preliminary estimation of engine gas-flow-path size and weight," *Journal of Propulsion and Power*, vol. 14, no. 2, pp. 208–214, 1998, ISSN: 0748-4658. DOI: 10.2514/2.5269.

[29] L. R. Jenkinson, P. Simpkin, and D. Rhodes, *Civil Jet Aircraft Design*. Arnold, a member of the Hodder Headline Group and American Institute of Aeronautics and Astronautics, 1999, 445 pp.

[30] C. Svoboda, "Turbofan engine database as a preliminary design tool," *Aircraft Design*, vol. 3, no. 1, pp. 17–31, 2000, PII: S136988699900021X, ISSN: 13698869. DOI: 10.1016/S1369-8869(99)00021-X.

[31] A. Guha, D. Boylan, and P. Gallagher, "Determination of optimum specific thrust for civil aero gas turbine engines: A multidisciplinary design synthesis and optimisation," *Proceedings of the Institution of Mechanical Engineers, Part G: Journal of Aerospace Engineering*, vol. 227, no. 3, pp. 502–527, 2013, ISSN: 0954-4100. DOI: 10.1177/0954410011435623.

[32] G. B. Pantalone, "Development of an engine model for an integrated aircraft design tool," Department of Aeronautics and Astronautics, Master Thesis, Massachusetts Institute of Technology, 2015.

[33] E. Onat and G. W. Klees, *A method to estimate weight and dimensions of large and small gas turbine engines*, Final Report, NASA, 1979.

[34] P. L. Hale, *A method to estimate weight and dimensions of small aircraft propulsion gas turbine engines, Final report and user's guide*, NASA, 1982.

[35] M. T. Tong, I. Halliwell, and L. J. Ghosn, "A computer code for gas turbine engine weight and disk life estimation," in *Proceedings of the ASME Turbo Expo 2002, Presented at the 2002 ASME Turbo Expo, June 3 - 6, 2002, Amsterdam, the Netherlands*, (Amsterdam, The Netherlands,), American Society of Mechanical Engineers and International Gas Turbine Institute, New York, NY: American Society of Mechanical Engineers, 2002, pp. 111–118, ISBN: 0-7918-3606-1. DOI: 10.1115/GT2002-30500.

[36] E. M. Greitzer *et al.*, *N+3 aircraft concept designs and trade studies, final report, Volume 2: Appendices—design methodologies for aerodynamics, structures, weight, and thermodynamic cycles*, Cleveland, Ohio 44135: NASA Glenn Research Center, 2010.

[37] M. T. Tong, I. Halliwell, and L. J. Ghosn, "A computer code for gas turbine engine weight and disk life estimation," *Journal of Engineering for Gas Turbines and Power*, vol. 126, no. 2, pp. 265–270, 2004, ISSN: 0742-4795. DOI: 10.1115/1.1691980.

[38] A. J. B. Jackson, "Optimisation of aero and industrial gas turbine design for the environment," School of Engineering, Dissertation, Cranfield University, 2009, 265 pp.

[39] E. Hendricks and M. Tong, "Performance and weight estimates for an advanced open rotor engine," in *48th AIAA/ASME/SAE/ASEE Joint Propulsion Conference & Exhibit*, (Atlanta, Georgia), Reston, Virigina: American Institute of Aeronautics and Astronautics, 7302012, ISBN: 978-1-60086-935-8. DOI: 10.2514/6.2012-3911.

[40] "Icao aircraft engine emissions databank." version v28c, European Union Aviation Safety Agency. (2021), [Online]. Available: https://www.easa.europa.eu/domains/environment/icao-aircraft-engine-emissions-databank#group-easa-downloads (visited on 05/14/2022).

[41] J. Kurzke, "Fundamental differences between conventional and geared turbofans," in *Proceedings of the ASME Turbo Expo 2009, Presented at the 2009 ASME Turbo Expo, June 8 - 12, 2009, Orlando, Florida, USA*, (Orlando, Florida, USA,), American Society of Mechanical Engineers and International Gas Turbine Institute, New York, NY: ASME, 2009, pp. 145–153, ISBN: 978-0-7918-4882-1. DOI: 10.1115/GT2009-59745.

[42] "Technische daten pw1100g-jm, mtu aero engines." (), [Online]. Available: https://www.mtu.de/de/maintenance/customized-solutions-for-aero-engines/engine-portfolio-mro/narrowbody-and-regional-jets/pw1100g-jm/ (visited on 05/14/2022).

[43] *Type-certificate data sheet no. im.e.093, Pw1100g-jm series engines*, European Union Aviation Safety Agency, 2019.

[44] M. Borg. "The pratt & whitney pw1000g engine family, Past, present and future for gkn aerospace," GKN Aerospace. (2016), [Online]. Available: https://ftfsweden.se/wp-content/uploads/2016/11/FT2016_A12_Borg.pdf (visited on 05/19/2022).

[45] M.-T. Perez-Prado and M. E. Kassner, “Creep of intermetallics,” in *Fundamentals of Creep in Metals and Alloys*, Elsevier, 2015, pp. 189–232, ISBN: 9780080994277. DOI: 10.1016/B978-0-08-099427-7.00009-8.

[46] “Backgrounder titanaluminid,” MTU Aero Engines. (2016), [Online]. Available: https://www.mtu.de/fileadmin/DE/7_News_Media/1_Presse/3_Pressekits/ILA_2016/Backgrounder/Backgrounder_Titaniumaluminide_DEU.pdf (visited on 05/20/2022).

[47] H. Grieb, Ed., *Projektierung von Turboflugtriebwerken*, ger, Technik der Turboflugtriebwerke, Grieb, Hubert (VerfasserIn), Basel and s.l.: Birkhäuser Basel, 2004, 826 pp., ISBN: 978-3-0348-9627-6. DOI: 10.1007/978-3-0348-7938-5.